Evolutionary integration and modularity in the archosaur cranium

Felice, R. N.[1,2], Watanabe, A.[2,3,4], Cuff, A.R.[5], Noirault, E.[2], Pol, D.[6], Witmer, L. M.[7], Norell, M.A.[4], O'Connor, P.M.[7,8], Goswami, A.[2]

[1]Centre for Integrative Anatomy, Department of Cell and Developmental Biology, University College London, London WC1E 6BT, UK

[2]Life Sciences Department, Vertebrates Division, Natural History Museum, London, SW7 5BD, UK

[3]Department of Anatomy, New York Institute of Technology College of Osteopathic Medicine, Old Westbury, NY 11568, USA

[4]Division of Paleontology, American Museum of Natural History, New York, NY 10024, USA

[5]Structure and Motion Laboratory, Department of Comparative Biomedical Sciences, Royal Veterinary College, Hawkshead Lane, North Mymms, Hertfordshire, AL9 7TA, United Kingdom.

[6]CONICET. Museo Paleontológico Egidio Feruglio, Av. Fontana 140, U9100GYO Trelew, Chubut, Argentina

[7]Department of Biomedical Sciences, Ohio University Heritage College of Osteopathic Medicine, Athens, Ohio, United States of America

[8]Ohio Center for Ecology and Evolutionary Studies, Ohio University, Athens, Ohio, United States of America

Abstract

Complex structures, like the vertebrate skull, are composed of numerous elements or traits that must develop and evolve in a coordinated manner to achieve multiple functions. The strength of association among phenotypic traits (i.e., integration), and their organization into highly-correlated, semi-independent subunits termed modules, is a result of the pleiotropic and genetic correlations that generate traits. As such, patterns of integration and modularity are thought to be key factors constraining or facilitating the evolution of phenotypic disparity by influencing the patterns of variation upon which selection can act. It is often hypothesized that selection can reshape patterns of integration, parceling single structures into multiple modules or merging ancestrally semi-independent traits into a strongly correlated unit. However, evolutionary shifts in patterns of trait integration are seldom assessed in a unified quantitative framework. Here, we quantify patterns of evolutionary integration among regions of the archosaur skull to investigate whether patterns of cranial integration are conserved or variable across this diverse group. Using high-dimensional geometric morphometric data from 3D surface scans and CT scans of modern birds (n=352), fossil non-avian dinosaurs (n=27), and modern and fossil mesoeucrocodylians (n=38), we demonstrate that some aspects of cranial integration are conserved across these taxonomic groups, despite their major differences in cranial form, function, and development. All three groups are highly modular and consistently exhibit high integration within the occipital region. However, there are also substantial divergences in correlation patterns. Birds uniquely exhibit high correlation between the pterygoid and quadrate, components of the cranial kinesis apparatus, whereas the non-avian dinosaur quadrate is more closely associated with the jugal and quadratojugal. Mesoeucrocodylians exhibit a slightly more integrated facial skeleton overall than the other grades. Overall, patterns of trait integration are shown to be stable among archosaurs, which is surprising given the cranial diversity exhibited by the clade. At the same time, evolutionary innovations such as

cranial kinesis that reorganize the structure and function of complex traits can result in modifications of trait correlations and modularity.

Introduction

The evolution of multi-functional structures requires that the associations among and within complex traits can shift in response to natural selection, gaining new phenotypes and functions. This is exemplified by the evolution of the vertebrate skull. For example, the exaptation of pharyngeal arches to form the jaw (Miyashita 2016) and the evolution of the mammalian middle ear from post-dentary mandibular bones (Urban et al. 2017) illustrate qualitatively how patterns of correlations among traits can shift as new functions evolve. These types of shifting associations among traits are possible because of both the integration of traits and the modular nature of complex phenotypes. Morphological integration describes the strength and patterns of correlation among traits, while modularity describes the degree to which clusters of highly-integrated traits form semi-independent subunits (Olson and Miller 1958). Patterns of integration and modularity among phenotypic traits reflect the underlying developmental and genetic systems that generate the traits (Wagner and Altenberg 1996; Klingenberg 2008; Goswami et al. 2009; Hallgrímsson et al. 2009; Wagner and Zhang 2011). Thus, by quantifying the strength and pattern of phenotypic modularity, it is possible to gain insight into the systems generating variation and, in turn, the evolution of the structures in question (Hansen and Houle 2008; Klingenberg and Marugán-Lobón 2013; Goswami et al. 2014; Felice et al. 2018).

The effect of trait correlation on macroevolution can vary, either facilitating or constraining phenotypic evolution, depending on the direction of selection on correlated traits (Goswami et al. 2014; Felice et al. 2018). Trait correlation determines the axes of variation and thus the “lines of least resistance” upon which selection can act. When selection is aligned with the major axis of variation, integrated traits can promote higher morphological disparity than unintegrated structures (Goswami et al. 2014). In contrast, when there is discordant selection on the sub-units comprising an integrated whole, the evolutionary response may be constrained. Patterns of integration and modularity are thought to evolve (Wagner and Altenberg 1996; Goswami et al. 2015). However, most studies of evolutionary modularity have focused on single clades and do not assess shifting patterns of trait correlation (although see Goswami 2006; Piras et al. 2014; Haber 2015; Anderson et al. 2016; Heck et al. 2018). The tetrapod skull has been one of the most common structures used to studying phenotypic modularity. Most analyses have focused on testing simple or single hypotheses of modularity. Typically, this involves quantifying the strength of correlation between the face and braincase regions of the skull (Marugán-Lobón and Buscalioni 2003; Kulemeyer et al. 2009; Klingenberg and Marugán-Lobón 2013; Piras et al. 2014; Bright et al. 2016). However, evidence from mammals (Cheverud 1982, 1995, 1996; Marroig and Cheverud 2001; Goswami 2006; Porto et al. 2009, 2009; Santana and Lofgren 2013; Goswami and Finarelli 2016; Parr et al. 2016), lizards (Sanger et al. 2012), birds (Felice and Goswami 2018), and caecilians (Bardua et al. 2019; Marshall et al. 2019) indicate that the patterns of trait covariation in the skull are much more complex than can be accurately summarized with these two-module hypotheses based on a limited sampling of anatomical landmarks.

Recent advances in geometric morphometric techniques have allowed complex phenotypes to be quantified with higher detail than before (Botton-Divet et al. 2015; Parr et al. 2016; Fabre et al. 2018; Felice and Goswami 2018; Martınez-Abadıas et al. 2018; Bardua et al. 2019). At the same time, new approaches for testing hypotheses of modularity have allowed for more complex hypotheses of modularity to be evaluated using these data (Márquez 2008; Adams 2016; Goswami and Finarelli 2016; Larouche et al. 2018). Using high-dimensional geometric morphometrics, we recently quantified the strength of correlation among the components of the avian skull, demonstrating that the avian cranium is highly modular (Felice and Goswami 2018). All skull regions exhibit relatively weak correlations with each other except for the jaw joint and pterygoid, which show a high level of integration. Our approach revealed that each cranial module evolves with a unique tempo and mode and are variably associated with trophic ecology (Felice and Goswami 2018; Felice et al. 2019). However, it is unclear whether the particular pattern of trait correlations in the avian skull represents a pattern unique to birds or if this pattern was inherited from their non-avian dinosaur ancestors. In addition, the highly fused nature of the avian skull obscures the boundaries between many of the cranial elements (e.g., nasal and premaxilla, frontal and parietal). This fusion limits the potential to further subdivide landmark configurations quantifying the avian skull into smaller units for testing more complex hypotheses of modularity, like those that can be tested in many other vertebrates (Cheverud 1982; Goswami and Finarelli 2016; Bardua et al. 2019). For example, examining shape correlations between different bones, let alone the individual ossifications, that make up the cranial vault would be impossible. However, we can examine patterns of modularity in the close bird relatives that exhibit more distinct boundaries between cranial elements, including their closest living relatives, Crocodylia, and extinct non-avian dinosaurs.

Crocodylomorpha *(*crocodylians and their extinct relatives) represents the only extant archosaurs other than birds. Although much maligned for their apparent lack of ecological and morphological disparity, more recent studies have highlighted the previously underappreciated craniofacial and ecomorphological variation in Crocodylomorpha (Pierce et al. 2008; Stubbs et al. 2013; Wilberg et al. 2019). This is especially true of fossil forms like notosuchians and peirosaurids which exhibit more diverse dentition and trophic ecology than modern forms (e.g., Pierce et al. 2009; Sereno and Larsson 2009). Did crocodylomorphs achieve their high cranial diversity under the same pattern of integration and modularity as birds? Or have differences in skull function and development forged different trait organization in these taxa? Using 3D morphometrics, it has been shown that the face and braincase of extant crocodylians are strongly integrated, with stronger integration in Alligatoridae than Crocodylidae (Piras et al.

2014). However, these analyses have never before been extended to include the broader crocodylomorph or archosaur clades, nor have more complex modularity patterns been assessed.

Non-avian dinosaur skulls exhibit even larger cranial disparity than crocodylomorphs, exemplified by wide range of cranial ornaments, dentitions, and feeding systems. As the sole extant clade of dinosaurs, neoavian birds have undergone major developmental and structural reorganization of the skull, including restructuring of the face and vault (Bhullar et al. 2012, 2015; Maddin et al. 2016; Fabbri et al. 2017; Smith-Paredes et al. 2018). These types of developmental shifts are expected to change patterns of cranial integration and modularity. However, very little is known about cranial integration in non-avian dinosaurs. Data from linear measurements have suggested that the face, orbit, and braincase are independently evolving modules in dinosaurs (Marugán-Lobón and Buscalioni 2003), but this has yet to be tested with modern morphometric approaches.

Here, we quantify the cranial integration and modularity across archosaur groups using unprecedented 3D geometric morphometric data for these groups and unprecedented taxonomic sampling. By comparing the patterns of trait covariation observed across Dinosauria and in Crocodylomorpha, we evaluate whether patterns of cranial integration have remained static through the nearly 250-million-year history of archosaurs or evolved with changes in skull structure, function, and development.

Methods

Morphometric Data

We quantified skull morphology across archosaurs using 3D digital models derived from surface scans and CT scans of modern and fossil specimens. For fossil specimens, we selected only those that were highly complete, articulated, and undeformed or had the ability to be retrodeformed (i.e., taphonomic deformation removed by editing digital model of the specimen). Although this requirement constrains our overall taxonomic sampling, it limits the effects of taphonomy and missing data on the results. Our dataset is composed of 352 extant bird species, 24 extant and 14 extinct mesoeucrocodylian crocodylomorph species, and 27 extinct non-avian dinosaurs (Electronic Supplementary Material 1). We focus on evolutionary (i.e., interspecific) modularity and integration rather than static (i.e. intraspecific variation within a growth stage) modularity and integration as few extinct archosaurs are known from enough cranial specimens for rigorous morphometric analysis at this resolution. Furthermore, studying evolutionary integration and modularity with broad taxonomic sampling and fossil data, as in the present dataset, allows for the study of shifts in trait correlation patterns in deep time (Klingenberg 2014; Goswami et al. 2015). For each group, we established a landmarking scheme allowing for the maximum number of anatomically distinct regions to be partitioned given the presence of visible sutures in the digitized data (Electronic Supplementary Material 2). For mesoeucrocodylians and non-avian dinosaurs, the premaxilla, maxilla, nasal, frontal, parietal, squamosal, prefrontal+ lacrimal, jugal+quadratojugal, postorbital, supraoccipital/exoccipital/otoccipital, occipital condyle, basioccipital, and articular surface of the quadrate are preserved in all specimens. In mesoeucrocodylians, the pterygoid, ectopterygoid, pterygoid flange, palatine, ventral surface of the maxilla and ventral surface of the premaxilla were also quantified. However, the ventral surface of the skull is preserved and accessible in fewer than 30% (9 of 27 species) of the non-avian dinosaur specimens. Thus, these regions were excluded from the non-avian dinosaur dataset. Furthermore, many of the non-avian dinosaur species are preserved with the cervical vertebrae and/or mandible in articulation with the skull, obscuring the occipital and jaw joint regions. For this reason, we divided the dinosaur dataset into two groups. One that contains 27 species which preserve nine regions on the lateral and dorsal elements of the skull (premaxilla, maxilla, nasal, frontal, prefrontal+lacrimal, parietal, squamosal, jugal+quadratojugal, and postorbital). The second dataset is made up of the 19 of these 27 specimens which also preserve the anatomy of the occipital region (supraoccipital, occipital condyle, basioccipital) and the articular surface of the quadrate. These datasets (the 9-region dataset and 13-region dataset respectively) represent our effort to optimize specimen number and anatomical sampling.

Compared to mesoeucrocodylians and non-avian dinosaurs, crown birds have highly fused skulls with fewer visible cranial sutures present in adults (Baumel and Witmer 1993; Bhullar et al. 2015; Maddin et al. 2016; Fabbri et al. 2017). Therefore, anatomical landmarks at the sutural boundaries of all the regions present in the other groups are difficult to discern. We employed a previously described landmarking scheme for the bird dataset that divides the skull into the rostrum, palate, vault, occipital, basisphenoid, pterygoid, naris, and articular surface of the quadrate (Felice and Goswami 2018).

Whereas anatomical landmarks and boundaries marked by semilandmarks can provide a robust characterization of anatomical structures (Gunz et al. 2005), these points are largely limited to the contact between, or midlines of, elements. Hence, this approach thus excludes large portions of anatomical variation that exists within complex cranial regions. For example, many pachycephalosaurs exhibit ornamental horns on the squamosal which would not be captured by simple semilandmark curves around the margins of the squamosal (Goodwin and Evans 2016). In this study, we used a semi-automated procedure, implemented in the R package “Morpho” to project surface semilandmarks from a template on to each specimen (Schlager 2017). This results in a high-dimensional morphometric characterization of surficial shape of the skull (Figure 1).

Anatomical landmarks were digitized on the left and right sides, but semilandmark curves and surface semilandmarks were digitized on the right side due to the frequency of incompletely preserved fossil specimens. Digital models of specimens which show better preservation on the left side were mirrored before landmarking. Finally, for each group, right-side semilandmarks were mirrored to the left side to mitigate artifacts related to Procrustes alignment of unilateral points on symmetrical structures (Cardini 2016). After subjecting each dataset to Procrustes alignment, all left-side landmarks were removed to reduce the dimensionality of the data and remove redundancy in shape information due to bilateral symmetry. The final datasets consist of 757 landmarks and semi-landmarks in birds, 1515 landmarks and semi-landmarks in non-avian dinosaurs, and 1291 landmarks and semi-landmarks for mesoeucrocodylians.

Phylogenetic Hypotheses

To evaluate the strength of correlation between skull regions, we employed phylogenetically informed analysis of modularity by calculating the independent contrasts of shape and calculating trait correlations on these data (Felsenstein 1985). For the bird dataset, we utilized a phylogenetic hypothesis that combines the backbone topology of a recent molecular sequencing dataset (Prum et al. 2015) to which the fine-scale relationships of an older species-level topology (Jetz et al. 2012) were grafted. This topology was generated following published procedures (Cooney et al. 2017) and has been used extensively to study avian macroevolution in recent years (Chira et al. 2018; Felice and Goswami 2018; Felice et al. 2019).

The relationships among non-avian dinosaurs are currently debated, with the uncertainty focused on the branching of Theropoda, Sauropodomorpha, and Ornithischia. Traditionally, Theropoda and Sauropodomorpha form a monophyletic clade (Saurischia) (Steeley 1887; Langer and Benton 2006; Nesbitt 2011; Langer et al. 2017). In contrast, some recent hypotheses have placed Ornithischia as the sister clade to Theropoda (forming Ornithoscelida)

(Baron et al. 2017; Müller and Dias-da-Silva 2017; Parry et al. 2017). We performed analyses on non-avian dinosaurs with two phylogenetic trees—a "traditional" topology with Theropoda and Sauropodomorpha as Saurischia and another with "Ornithoscelida". The time-calibrated "traditional" topology was generated using first and last appearance data to calibrate the phylogeny in the R package "paleotree" (Bapst 2012), generating a posterior distribution of dated tree (e.g., Benson and Choiniere 2013). We then used TreeAnnotator to create a maximum clade credibility tree from this distribution (Drummond et al. 2012). To create the Ornithoscelida topology, we manually manipulated the basal branches from the "traditional" topology to match the published undated phylogenies originally reported for the hypothesis (Baron et al. 2017).

There are two main areas of uncertainty in the phylogenetic relationships of Crocodylomorpha. These relate to the affinities of the false gharial (*Tomistoma schlegelii*) and the marine thalattosuchians. *Tomistoma* has been reconstructed as either a sister to *Gavialis gangeticus* (Gatesy et al. 2003; Willis et al. 2007) or as a member of Crocodylidae (Brochu 1997, 2003), whereas Thalattosuchia may be nested within Neosuchia (Pol and Gasparini 2009) or basal to Crocodyliformes (Benton and Clark 1988; Wilberg 2015). Because of these debated relationships, we conducted all analyses of mesoeucrocodylians with 4 different topologies, representing the four possible combinations of these hypotheses. Trees were time calibrated applying the same methods used for non-avian dinosaurs (Electronic Supplemental Data 3).

Modularity

We evaluated the strength of correlation among cranial regions using two methods. First, we used the EMMLi method, a likelihood-based approach which allows multiple hypotheses of modular organization to be compared (Goswami and Finarelli 2016). This is achieved by calculating model likelihood from the within- and between-module correlations (ρ) for alternative hypotheses. For each dataset, we tested multiple hypotheses of cranial organization (Electronic supplemental Data Table 4), ranging from the entire skull as a single module, to two modules (face and neurocranium) to all cranial elements as modules (19 modules in mesoeucrocodylians, 13 modules in non-avian dinosaurs, and 8 modules in birds, Fig. 1). Second, we used covariance ratio (CR) analysis implemented in the “geomorph” R package (Adams and Otárola-Castillo 2013) to quantify the strength of association between modules with a measure derived from the covariance matrix of the traits and to evaluate significance using a permutation procedure (Adams 2016). Both analyses were conducted in a phylogenetically-informed context with each of the topologies described above by performing the analyses on the phylogenetic independent contrasts of shape, calculated using the “ape” R package (Felsenstein 1985; Paradis et al. 2004).

To test whether allometric effects significantly affect skull shape and integration patterns, we conducted a Procrustes linear regression against log-transformed centroid size (Collyer et al. 2015). In birds ($R^2 = 0.18$, $p < 0.001$) and mesoeucrocodylians ($R^2 = 0.22$, $p < 0.001$), allometry has a small but significant effect on shape, but the effects of allometry are non-significant in non-avian dinosaurs (13 region dataset: $R^2 = 0.07$, $p = 0.299$; 9 region dataset: $R^2 = 0.06$, $p = 0.127$). Following this result, we carried out EMMLi analyses on the size-corrected shape data derived from the residuals of the linear regression for the bird and mesoeucrocodylian datasets.

We repeated the phylogenetically-informed EMMLi analysis on the mesoeucrocodylian data with landmarks partitioned into just seven regions corresponding to the regions present in the bird dataset to allow direct comparability between analyses of these clades. To ensure that differences in pattern of modularity were not due to differences in dimensionality of the landmark configurations, we randomly subsampled the mesoeucrocodylian data to contain the same number of landmarks as the bird data using the subsampleEMMLi function in the “EMMLiv2” R package (www.github.com/hferg/EMMLiv2). Subsampling was repeated for 100 iterations. The basisphenoid has little to no exposure on the external cranial surface in mesoeucrocodylians and was thus excluded from this analysis.

RESULTS:

In all EMMLi analyses, the hypothesis with the highest number of regions had the highest likelihood (Electronic Supplementary Data 5A-N). These modularity hypotheses are also supported by CR analysis (Electronic Supplementary Data 5O-R). The choice of phylogenetic topology does not appreciably alter the patterns of modularity and integration. Thus, we present the results using the traditional Dinosauria phylogenetic topology and Crocodylomorpha hypothesis 1 (thalattosuchians as neosuchians and *Tomistoma* as Crocodylidae) here and the results for all other topologies in the Electronic Supplemental Data 5. In birds, non-avian dinosaurs, and mesoeucrocodylians, all regions in the most-parameterized modularity hypothesis are significantly modular (CR < 1, p<0.001). Examination of the correlations among regions demonstrated that birds exhibit weak correlation between all cranial regions except for the articular part of the quadrate and the pterygoid (Fig. 2A, Electronic Supplementary Data 5E). The correlation between these two elements (ρ = 0.63) is greater than the maximum within-region correlation of any of the 8 regions present (basisphenoid, ρ = 0.62). In contrast, the pterygoid and quadrate are weakly correlated in mesoeucrocodylians (ρ = 0.18, Fig 2C, Electronic Supplementary Data 5F-I) relative to within-region correlation in these structures (pterygoid: ρ = 0.69, quadrate: ρ = 0.95). Instead, mesoeucrocodylians exhibit the highest correlations between occipital components (occipital condyle to supraoccipital: ρ = 0.57, occipital condyle to basioccipital: ρ = 0.60) and the dorsal and ventral sides of the premaxilla (ρ = 0.74). The frontal and prefrontal/lacrimal complex also exhibit high correlation in mesoeucrocodylians (ρ = 0.56).

When EMMLi is applied to the mesoeucrocodylian dataset with the same modularity hypothesis observed in birds, some important similarities and differences between these clades are observed (Fig. 2C). In both birds and mesoeucrocodylians, the vault and occipital region exhibit weak correlations with each other and with all other regions (Electronic Supplementary Data 5J-M). Unlike birds, mesoeucrocodylians exhibit the highest correlation between the anterior and ventral elements of the skull (rostrum, palate, naris, pterygoid, and articular part of the quadrate). However, all between-module correlations (ρ = 0.23-0.35) are much lower than the lowest within-module correlation value (naris, ρ = 0.50), indicating relative decoupling of these skull regions with respect to shape variation.

In non-avian dinosaurs, the correlations between elements of the occipital region are high (ρ = 0.59-0.82), as in mesoeucrocodylians (Fig 2D, Electronic Supplementary Data 5). Unlike mesoeucrocodylians, however, the quadrate is strongly correlated with the jugal+quadratojugal region (ρ = 0.72) in non-avian dinosaurs. All other pairwise comparisons of skull regions show relatively low correlations (rho < 0.50). In the 9-region dataset which excludes the quadrate and occipital region, there is high within-region correlation (ρ = 0.69-0.82, Electronic Supplemental Data 5A-D) and relatively low between-module correlation. The strongest between-region correlation are observed between the premaxilla and maxilla (ρ = 0.43), premaxilla and nasal (ρ = 0.47), parietal and frontal (ρ = 0.46), and the postorbital with the squamosal and lacrimal/prefontal (ρ = 0.43). This result suggests that rostral elements (premaxilla, maxilla, nasal) and the neurocranium (parietal, frontal, postorbital, squamosal) are highly integrated, and these are in fact fused structures in birds.

Effects of Allometry:

Evolutionary (interspecfic) allometry has been proposed as a significant factor shaping phenotypic integration in the avian skull (Bright et al. 2016). Our analysis shows that allometry has relatively minor effects on patterns of trait correlations. In birds, within- and between-region correlations are reduced by as much as 52% when allometric size is removed from the shape data (Electronic Supplementary Data 5E). However, relative patterns of correlation remain the same, with the highest within-region correlation in the pterygoid, basisphenoid, and quadrate and the highest between-region correlation between the pterygoid and quadrate. This finding indicates that allometric size is a significant factor driving the magnitude of, but not overall patterns of, modularity and integration in birds. Whereas allometry contributes to stronger trait correlation in birds, the effect of allometry is more complex in mesoeucrocodylians (Electronic Supplementary Data 5E). Allometry tends to contribute to stronger correlation between the occipital condyle and the lacrimal/prefrontal regions with other regions of the cranium. Conversely, the ectopterygoid, pterygoid, pterygoid flange, and jugal+quadratojugal are less strongly correlated with other skull regions as a result of allometry. Taken together, the overall pattern of modularity is similar with and without the effects of allometric size, with the highest correlations between the parts of the premaxilla and between the ectopterygoid and pterygoid flange. However, occipital elements are not strongly correlated when the effect of allometry on shape is statistically removed. This finding indicates that size drives the integration of the basicranium in mesoeucrocodylians, which reflect the scaling of biomechanical forces related to the loads produced by larger heads.

Discussion:

Birds and their relatives show distinct patterns of trait correlation across the skull. In birds, the strongest correlations are between the quadrate and pterygoid, articulated elements that contribute to cranial kinesis (Bock 1964). Within-region correlation is highest in neurocranial and basicranial elements compared to the face and palate. If this pattern of modularity were inherited from non-avian dinosaurs, we expect the non-avian dinosaurs to exhibit high between-element correlation in these bones. Indeed, the supraoccipital, basioccipital, and occipital condyle are strongly correlated in non-avian dinosaurs, as well as in the mesoeucrocodylian dataset. This shared pattern suggests that a highly integrated occipital is an ancestral feature of archosaurs. The occipital is a highly multifunctional skull region as the site of articulation of the skull to the vertebral column, attachment area for the cervical musculature, and transmission of the spinal cord. Tightly correlated evolution of this region may be essential to properly maintaining its many functions. Furthermore, the observation that occipital integration is partially related to allometric effects suggests that high integration is related to biomechanical function (i.e., supporting loads at the craniocervical junction). This is also consistent with the observation that the basicranium experiences slow or conserved evolutionary patterns in some clades (Polly et al. 2006).

Although assessing patterns of integration and modularity in the palate or pterygoid in non-avian dinosaurs is challenging with the current sample, we observe notable differences in palatal integration when comparing mesoeucrocodylians and birds. The premaxilla in mesoeucrocodylians exhibits high integration among its skull regions, but the maxilla does not. This correlation among the premaxillary regions is enough to generate relatively strong rostrum-palate correlation in mesoeucrocodylians, when landmarks are binned according to the regions present in birds. Notably in mesoeucrocodylians, the palatal surface of the pterygoid, the pterygoid flange, and the ectopterygoid are strongly correlated. This region not only forms the bony secondary palate but also forms an “open joint” which buttresses the mandibles (Ferguson 1981; Walmsley et al. 2013). As such, shifts in the integration of the pterygoid with other adjacent elements may be driven by divergence in pterygoid function. Data from early branching archosauromorphs and dinosauromorphs, as well as non-neornithine paravians, are needed to track palate and pterygoid shape evolution across Archosauria to determine whether birds or mesoeucrocodylians (or both) represent a deviation from the ancestral patterns of association in this cranial region.

One area where avian and non-avian dinosaurs diverge is in the strength of correlation between the quadrate and other elements. In non-avian dinosaurs, we recover a high correlation between the articular surface of the quadrate and the jugal+quadratojugal region. The quadratojugal is articulated posteriorly with the quadrate and both elements contribute to the shape of the inferior temporal fenestra. Consequently, the position of the articular surface of the quadrate is expected to show correlated evolution with the jugal region. Because of a lack of a clear suture between the maxilla and jugal in extant birds, the jugal and quadratojugal were included as part of the “rostrum” module of the skull. As a result, we cannot test whether the avian jugal bar is more correlated with the quadrate or with the anterior face given the current bird landmark configuration. The anatomy of the jugal and quadratojugal underwent massive changes through avian evolution, becoming a slender bar associated with the cranial kinesis system (Bock 1964; Wang and Hu 2017). Indeed, avian cranial kinesis is a multi-bar linkage system that incorporates articulation of the beak, jugal, pterygoid, quadrate, and squamosal (Bock 1964; Olsen and Westneat 2016). However, because of the fusion of sutures in the neurocranium and rostrum in crown birds, it was only possible to isolate the quadrate and pterygoid, which show high integration. It is not currently possible to test whether functional and anatomical changes among the other elements of this system resulted in changes in trait correlations (or vice versa). Answering this question will necessitate focused study on these specific elements in early birds and paravians.

The observed patterns of modularity and integration are detectable due to the high-dimensional geometric morphometric data used to quantify skull shape. This robust morphological characterization of each cranial element allows the strength of correlation between and within individual skull elements to be measured more accurately than with only Type I landmarks (Bookstein 1991). Critically, regional analysis in non-avian dinosaurs allowed for the detection of quadratojugal-quadrate integration, a deviation from previous findings in avian dinosaurs (Felice and Goswami 2018). This demonstrates how increasingly fine-scale partitioning of hypotheses for cranial organization can lead to the discovery of new patterns and drive new hypotheses. Moreover, the fused regions present in birds (e.g., rostrum, vault, occipital region) are composed of bones which exhibit high between-region correlations in non-avian dinosaurs. Therefore, the fusion observed in bird skulls are likely the result of enhancing existing patterns of trait correlation already present in non-avian dinosaurs.

Taken together, these findings illustrate that evolutionary grades within Archosauria exhibit largely congruent patterns of trait correlations across the skull. The differences across these groups in patterns of integration and modularity and integration are largely concentrated on the structures that form the palate and cranio-mandibular joint(s). This result adds to the growing body of evidence that patterns of integration are largely conserved within major clades but they are not immutable and can evolve (Goswami 2006; Piras et al. 2014; Haber 2015; Anderson et al. 2016; Heck et al. 2018). Because these groups differ so greatly in cranial disparity, geometry, mechanics, and development, a key next step is to investigate the causes of these shifts in trait correlations. The differences in craniofacial development that control modularity differences between birds and mesoeucrocrocodylians are only beginning to be understood (Bhullar et al. 2015; Maddin et al. 2016; Fabbri et al. 2017). Nonetheless, some major insights into craniofacial development in these clades are emerging as potential candidates for explaining integration patterns. For example, the evolution of the avian beak and palate phenotypes were achieved through shifts in the expression domains of the genes FGF and WNT in the frontonasal prominence during embryonic development (Bhullar et al. 2015). These evolutionary and developmental changes correspond with differences in phenotypic integration in the facial skeleton between birds and mesoeucrocodylians (low integration and high integration, respectively). As such, this restructuring of the developmental genetics and anatomy of the avian face and palate may have been responsible for the observed difference in integration. Similarly, superficially major differences in skull roof development and phenotype between birds and other tetrapods appear to be result of the morphogenic primacy of the brain over skull development (Fabbri et al. 2017). The relatively high within-neurocranium integration observed in birds, non-avian dinosaurs, and mesoeucrocodylians may be a consequence of underlying neuroanatomical integration patterns shaping the neurocranial elements examined in this study. The genetic and developmental underpinning of the pterygoid-quadrate correlation, however, remains to be seen.

Furthermore, understanding the macroevolutionary consequences of differences in cranial integration necessitates evolutionary model fitting using these data. In birds, integration constrains the evolution of disparity, as skull regions with higher within-module integration evolve at slower rates (Felice and Goswami 2018). Whether shifts in modularity across these three grades contribute to differences in evolutionary rates and disparity remains to be established. However, identifying differences in the patterns of cranial modularity across archosaurs is a critical step to investigating how modularity has shaped the evolution of diversity though deep time in this clade.

Acknowledgements

Thanks are due to those that contributed scan data: E. Rayfield, A. Knapp, D. Paluh, K. Melstrom, R. Sookias, J.M. Bourke, S. Baumgart, P.C. Sereno, and C. Early. Thanks also to the curators, and collections managers who facilitated specimen scanning: J. White, C. Lefevre, A. Herrel, C. Milensky, M. Brett-Surman, C. Mehling, D. Kizirian, A. Resetar, J. Maisano, P. Holroyd, S. Rogers, W. Simpson, B. Marks, J. Hinshaw, P. Sweet, L. Garetano, J. Rosado, K. Zyskowski, G. Watkins-Colwell, M. Ezcurra, A. Scarano, J Scanella, A. Henrici, B. Sanchez, B. Strilisky, C. Sidor, M. Rivin, and C. Levitt and to the organizers of the "Multifunctional structures and multistructural functions" Symposium.

Funding Statement:

This research was funded by European Research Council grant no. STG-2014-637171 (to A.G.) and SYNTHESYS grant no. FR-TAF-5635 (to R.N.F.). MAN's work was funded by the Macaulay family endowment to the AMNH, and NSF DEB-1457181. LMW's work was funded by NSF IOS-1050154 and IOS-1456503.

Author Contributions:

Analyses were designed by RNF, AW, and AG, and carried out by RNF and AG. All authors collected data and contributed to the writing of the manuscript.

Figure Captions:

Figure 1: Cranial regions in birds (dorsal, A; lateral, B; ventral, C), mesoeucrocodylians (dorsal, D; lateral, E; ventral, F), and non-avian dinosaurs (dorsal, G; lateral, H) characterized in this study. Three-dimensional surface semilandmarks were placed on digital skull models using the "Morpho" R package (Schlager 2017). Colors of landmarks indicate the cranial region based on the most parameterized model of modularity for that group. Landmarks are illustrated on *Pandion haliaetus* (USNM 623422, A-C) *Alligator mississippiensis* (AMNH R-40582, D-F) and *Erlikosaurus andrewsi* (IGM 100/111, G-H).

Figure 2: Networks diagrams illustrating the results of phylogenetically-informed EMMLi analyses. Nodes represent cranial regions, with the size of the circle scaled to the magnitude of within-region correlation. Lines connecting nodes represent the strength of correlation between regions, with darker, thicker lines representing higher correlation. Network plots are illustrated for birds (A), mesoeucrocodylians (B), mesoeucrocodylians with landmarks partitioned according to the regions present in birds (C), and non-avian dinosaurs (D). BOcc: basioccipital, Bsph: basisphenoid region, Co: occipital condyle, Ept: ectopterygoid, Fr: frontal, Jug: jugal and quadratojugal, Pf-Lac: lacrimal and prefrontal, Max(d): dorsolateral side of the maxilla, Max(v): ventral surface of maxilla, Na: nasal, Occ: occipital region, Pa: Parietal, Pal: palatine, P: palate region, PMax(d): dorsolateral side of the premaxilla, PMax(v): ventral surface of premaxilla, Po: postorbital, Pt: pterygoid, PtFl: pterygoid flange, Qu: articular surface of the quadrate, Ro: rostrum region, SOcc: superior occipital region including supraoccipital and otoccipital, Sq: squamosal.

References

Adams DC. 2016. Evaluating modularity in morphometric data: challenges with the RV coefficient and a new test measure. Methods in Ecology and Evolution 7:565–72.

Adams DC, Otárola-Castillo E. 2013. geomorph: an R package for the collection and analysis of geometric morphometric shape data. Methods in Ecology and Evolution 4:393–99.

Anderson PSL, Smith DC, Patek SN. 2016. Competing influences on morphological modularity in biomechanical systems: a case study in mantis shrimp: Morphological covariation. Evolution & Development 18:171–81.

Bapst DW. 2012. paleotree : an R package for paleontological and phylogenetic analyses of evolution. Methods in Ecology and Evolution 3:803–7.

Bardua C, Wilkinson M, Gower DJ, Sherratt E, Goswami A. 2019. Morphological evolution and modularity of the caecilian skull. BMC Evolutionary Biology 19.

Baron MG, Norman DB, Barrett PM. 2017. A new hypothesis of dinosaur relationships and early dinosaur evolution. Nature 543:501–6.

Baumel JJ, Witmer LM. 1993. Osteologia. In: Baumel JJ, editor. Handbook of avian anatomy: nomina anatomica avium Cambridge, Massachusetts: Publications of the Nuttall Ornithological Club. p. 45–132.

Benson RBJ, Choiniere JN. 2013. Rates of dinosaur limb evolution provide evidence for exceptional radiation in Mesozoic birds. Proceedings of the Royal Society B: Biological Sciences 280:20131780.

Benton MJ, Clark JM. 1988. Archosaur phylogeny and the relationships of the Crocodylia. In: Benton MJ, editor. The Phylogeny and Classification of the Tetrapods, Volume 1: Amphibians, Reptiles, Birds. Systematics Association Special Volume Oxford: Clarendon Press. p. 295–338.

Bhullar B-AS, Marugán-Lobón J, Racimo F, Bever GS, Rowe TB, Norell MA, Abzhanov A. 2012. Birds have paedomorphic dinosaur skulls. Nature 487:223–26.

Bhullar B-AS, Morris ZS, Sefton EM, Tok A, Tokita M, Namkoong B, Camacho J, Burnham DA, Abzhanov A. 2015. A molecular mechanism for the origin of a key evolutionary innovation, the bird beak and palate, revealed by an integrative approach to major transitions in vertebrate history. Evolution 69:1665–77.

Bock WJ. 1964. Kinetics of the avian skull. Journal of Morphology 114:1–41.

Bookstein FL. 1991. Morphometric tools for landmark data: geometry and biology Cambridge: Cambridge University Press.

Botton-Divet L, Houssaye A, Herrel A, Fabre A-C, Cornette R. 2015. Tools for quantitative form description; an evaluation of different software packages for semi-landmark analysis. PeerJ 3:e1417.

Bright JA, Marugán-Lobón J, Cobb SN, Rayfield EJ. 2016. The shapes of bird beaks are highly controlled by nondietary factors. Proceedings of the National Academy of Sciences 113:5352–57.

Brochu CA. 1997. Morphology, fossils, divergence timing, and the phylogenetic relationships of *Gavialis*. Systematic Biology 46:479–522.

Brochu CA. 2003. Phylogenetic approaches toward crocodylian history. Annual Review of Earth and Planetary Sciences 31:357–97.

Cardini A. 2016. Lost in the other half: improving accuracy in geometric morphometric analyses of one side of bilaterally symmetric structures. Systematic Biology 65:1096–1106.

Cheverud JM. 1982. Phenotypic, genetic, and environmental morphological integration in the cranium. Evolution 36:499–516.

Cheverud JM. 1995. Morphological integration in the saddle-back tamarin (*Saguinus fuscicollis*) cranium. The American Naturalist 145:63–89.

Cheverud JM. 1996. Developmental integration and the evolution of pleiotropy. American Zoologist 36:44–50.

Chira AM, Cooney CR, Bright JA, Capp EJR, Hughes EC, Moody CJA, Nouri LO, Varley ZK, Thomas GH. 2018. Correlates of rate heterogeneity in avian ecomorphological traits. Ecology Letters 21:1505–14.

Collyer ML, Sekora DJ, Adams DC. 2015. A method for analysis of phenotypic change for phenotypes described by high-dimensional data. Heredity 115:357–65.

Cooney CR, Bright JA, Capp EJR, Chira AM, Hughes EC, Moody CJA, Nouri LO, Varley ZK, Thomas GH. 2017. Mega-evolutionary dynamics of the adaptive radiation of birds. Nature 542:344–47.

Drummond AJ, Suchard MA, Xie D, Rambaut A. 2012. Bayesian phylogenetics with BEAUti and the BEAST 1.7. Molecular Biology and Evolution 29:1969–73.

Fabbri M, Mongiardino Koch N, Pritchard AC, Hanson M, Hoffman E, Bever GS, Balanoff AM, Morris ZS, Field DJ, Camacho J, Rowe TB, Norell MA, Smith RM, Abzhanov A, Bhullar B-AS. 2017. The skull roof tracks the brain during the evolution and development of reptiles including birds. Nature Ecology & Evolution 1:1543–50.

Fabre A-C, Perry JMG, Hartstone-Rose A, Lowie A, Boens A, Dumont M. 2018. Do muscles constrain skull shape evolution in strepsirrhines? The Anatomical Record 301:291–310.

Felice RN, Goswami A. 2018. Developmental origins of mosaic evolution in the avian cranium. Proceedings of the National Academy of Sciences 115:555–60.

Felice RN, Randau M, Goswami A. 2018. A fly in a tube: macroevolutionary expectations for integrated phenotypes. Evolution 72:2580–94.

Felice RN, Tobias JA, Pigot AL, Goswami A. 2019. Dietary niche and the evolution of cranial morphology in birds. Proceedings of the Royal Society B: Biological Sciences 286:20182677.

Felsenstein J. 1985. Phylogenies and the comparative method. The American Naturalist 125:1–15.

Ferguson MWJ. 1981. The structure and development of the palate in *Alligator mississippiensis*. Archives of Oral Biology 26:427–43.

Gatesy J, Amato G, Norell M, Desalle R, Hayashi C. 2003. Combined support for wholesale taxic atavism in gavialine crocodylians. Systematic Biology 52:403–22.

Goodwin MB, Evans DC. 2016. The early expression of squamosal horns and parietal ornamentation confirmed by new end-stage juvenile *Pachycephalosaurus* fossils from the Upper Cretaceous Hell Creek Formation, Montana. Journal of Vertebrate Paleontology 36:e1078343.

Goswami A. 2006. Cranial Modularity Shifts during Mammalian Evolution. The American Naturalist 168:270–80.

Goswami A, Binder WJ, Meachen J, O'Keefe FR. 2015. The fossil record of phenotypic integration and modularity: A deep-time perspective on developmental and evolutionary dynamics. Proceedings of the National Academy of Sciences 112:4891–96.

Goswami A, Finarelli JA. 2016. EMMLi: A maximum likelihood approach to the analysis of modularity. Evolution 70:1622–37.

Goswami A, Smaers JB, Soligo C, Polly PD. 2014. The macroevolutionary consequences of phenotypic integration: from development to deep time. Philosophical Transactions of the Royal Society B: Biological Sciences 369:20130254–20130254.

Goswami A, Weisbecker V, Sánchez-Villagra MR. 2009. Developmental modularity and the marsupial-placental dichotomy. Journal of Experimental Zoology Part B: Molecular and Developmental Evolution 312B:186–95.

Gunz P, Mitteroecker P, Bookstein FL. 2005. Semilandmarks in three dimensions. In: Slice DE, editor. Modern morphometrics in physical anthropology New York: Kluwer Academic Publishers-Plenum Publishers. p. 73–98.

Haber A. 2015. The evolution of morphological integration in the ruminant skull. Evolutionary Biology 42:99–114.

Hallgrímsson B, Jamniczky H, Young NM, Rolian C, Parsons TE, Boughner JC, Marcucio RS. 2009. Deciphering the palimpsest: studying the relationship between morphological integration and phenotypic covariation. Evolutionary Biology 36:355–76.

Hansen TF, Houle D. 2008. Measuring and comparing evolvability and constraint in multivariate characters. Journal of Evolutionary Biology 21:1201–19.

Heck L, Wilson LAB, Evin A, Stange M, Sánchez-Villagra MR. 2018. Shape variation and modularity of skull and teeth in domesticated horses and wild equids. Frontiers in Zoology 15:14.

Jetz W, Thomas GH, Joy JB, Hartmann K, Mooers AO. 2012. The global diversity of birds in space and time. Nature 491:444–48.

Klingenberg CP. 2008. Morphological integration and developmental modularity. Annual Review of Ecology, Evolution, and Systematics 39:115–32.

Klingenberg CP. 2014. Studying morphological integration and modularity at multiple levels: concepts and analysis. Philosophical Transactions of the Royal Society B: Biological Sciences 369:20130249–20130249.

Klingenberg CP, Marugán-Lobón J. 2013. Evolutionary covariation in geometric morphometric data: analyzing integration, modularity, and allometry in a phylogenetic context. Systematic Biology 62:591–610.

Kulemeyer C, Asbahr K, Gunz P, Frahnert S, Bairlein F. 2009. Functional morphology and integration of corvid skulls - a 3D geometric morphometric approach. Frontiers in Zoology 6:2.

Langer MC, Benton MJ. 2006. Early dinosaurs: A phylogenetic study. Journal of Systematic Palaeontology 4:309–58.

Langer MC, Ezcurra MD, Rauhut OWM, Benton MJ, Knoll F, McPhee BW, Novas FE, Pol D, Brusatte SL. 2017. Untangling the dinosaur family tree. Nature 551:E1–3.

Larouche O, Zelditch ML, Cloutier R. 2018. Modularity promotes morphological divergence in ray-finned fishes. Scientific Reports 8:7278.

Maddin HC, Piekarski N, Sefton EM, Hanken J. 2016. Homology of the cranial vault in birds: new insights based on embryonic fate-mapping and character analysis. Royal Society Open Science 3:160356.

Márquez EJ. 2008. A statistical framework for testing modularity in multidimensional data. Evolution 62:2688–2708.

Marroig G, Cheverud JM. 2001. A comparison of phenotypic variation and covariation patterns and the role of phylogeny, ecology, and ontogeny during cranial evolution of new world monkeys. Evolution 55:2576–2600.

Marshall AF, Bardua C, Gower DJ, Wilkinson M, Sherratt E, Goswami A. 2019. High-density three-dimensional morphometric analyses support conserved static (intraspecific) modularity in caecilian (Amphibia: Gymnophiona) crania. Biological Journal of the Linnean Society 22.

Martınez-Abadıas N, Estivill RM, Tomas JS, Perrine SM, Yoon M, Robert-Moreno A, Swoger J, Russo L, Kawasaki K, Richtsmeier J, Sharpe J. 2018. Quantification of gene expression patterns to reveal the origins of abnormal morphogenesis. eLife 7:e36405.

Marugán-Lobón J, Buscalioni ÁD. 2003. Disparity and geometry of the skull in Archosauria (Reptilia: Diapsida). Biological Journal of the Linnean Society 80:67–88.

Miyashita T. 2016. Fishing for jaws in early vertebrate evolution: a new hypothesis of mandibular confinement: Fishing for jaws. Biological Reviews 91:611–57.

Müller RT, Dias-da-Silva S. 2017. Taxon sample and character coding deeply impact unstable branches in phylogenetic trees of dinosaurs. Historical Biology 1–4.

Nesbitt SJ. 2011. The early evolution of archosaurs: relationships and the origin of major clades. Bulletin of the American Museum of Natural History 352:1–292.

Olsen AM, Westneat MW. 2016. Linkage mechanisms in the vertebrate skull: Structure and function of three-dimensional, parallel transmission systems. Journal of Morphology 277:1570–83.

Olson E, Miller R. 1958. Morphological integration Chicago: University of Chicago Press.

Paradis E, Claude J, Strimmer K. 2004. APE: Analyses of Phylogenetics and Evolution in R language. Bioinformatics 20:289–90.

Parr WCH, Wilson LAB, Wroe S, Colman NJ, Crowther MS, Letnic M. 2016. Cranial shape and the modularity of hybridization in dingoes and dogs; hybridization does not spell the end for native morphology. Evolutionary Biology 43:171–87.

Parry LA, Baron MG, Vinther J. 2017. Multiple optimality criteria support Ornithoscelida. Royal Society Open Science 4:170833.

Pierce SE, Angielczyk KD, Rayfield EJ. 2008. Patterns of morphospace occupation and mechanical performance in extant crocodilian skulls: A combined geometric morphometric and finite element modeling approach. Journal of Morphology 269:840–64.

Pierce SE, Angielczyk KD, Rayfield EJ. 2009. Morphospace occupation in thalattosuchian crocodylomorphs: skull shape variation, species delineation and temporal patterns. Palaeontology 52:1057–97.

Piras P, Buscalioni AD, Teresi L, Raia P, Sansalone G, Kotsakis T, Cubo J. 2014. Morphological integration and functional modularity in the crocodilian skull. Integrative Zoology 9:498–516.

Pol D, Gasparini Z. 2009. Skull anatomy of *Dakosaurus andiniensis* (Thalattosuchia: Crocodylomorpha) and the phylogenetic position of Thalattosuchia. Journal of Systematic Palaeontology 7:163–97.

Polly PD, Wesley-Hunt GD, Heinrich RE, Davis G, Houde P. 2006. Earliest known carnivoran auditory bulla and support for a recent origin of crown-group Carnivora (Eutheria, Mammalia). Palaeontology 49:1019–27.

Porto A, de Oliveira FB, Shirai LT, De Conto V, Marroig G. 2009. The evolution of modularity in the mammalian skull I: morphological integration patterns and magnitudes. Evolutionary Biology 36:118–35.

Prum RO, Berv JS, Dornburg A, Field DJ, Townsend JP, Lemmon EM, Lemmon AR. 2015. A comprehensive phylogeny of birds (Aves) using targeted next-generation DNA sequencing. Nature 526:569–73.

Sanger TJ, Mahler DL, Abzhanov A, Losos JB. 2012. Roles for modularity and constraint in the evolution of cranial diversity among *Anolis* lizards. Evolution 66:1525–42.

Santana SE, Lofgren SE. 2013. Does nasal echolocation influence the modularity of the mammal skull? Journal of Evolutionary Biology 26:2520–26.

Schlager S. 2017. Morpho and Rvcg – shape analysis in R. In: Statistical Shape and Deformation Analysis Elsevier. p. 217–56.

Sereno P, Larsson H. 2009. Cretaceous Crocodyliforms from the Sahara. ZooKeys 28:1–143.

Smith-Paredes D, Núñez-León D, Soto-Acuña S, O'Connor J, Botelho JF, Vargas AO. 2018. Dinosaur ossification centres in embryonic birds uncover developmental evolution of the skull. Nature Ecology & Evolution 2:1966–73.

Steeley HG. 1887. On the classification of the fossil animals commonly named Dinosauria. Proceedings of the Royal Society of London 43:165–71.

Stubbs TL, Pierce SE, Rayfield EJ, Anderson PSL. 2013. Morphological and biomechanical disparity of crocodile-line archosaurs following the end-Triassic extinction. Proceedings of the Royal Society B: Biological Sciences 280:20131940–20131940.

Urban DJ, Anthwal N, Luo Z-X, Maier JA, Sadier A, Tucker AS, Sears KE. 2017. A new developmental mechanism for the separation of the mammalian middle ear ossicles from the jaw. Proceedings of the Royal Society B: Biological Sciences 284:20162416.

Wagner GP, Altenberg L. 1996. Perspective: complex adaptations and the evolution of evolvability. Evolution 50:967.

Wagner GP, Zhang J. 2011. The pleiotropic structure of the genotype–phenotype map: the evolvability of complex organisms. Nature Reviews Genetics 12:204–13.

Walmsley CW, Smits PD, Quayle MR, McCurry MR, Richards HS, Oldfield CC, Wroe S, Clausen PD, McHenry CR. 2013. Why the long face? The mechanics of mandibular symphysis proportions in crocodiles. PLoS ONE 8:e53873.

Wang M, Hu H. 2017. A comparative morphological study of the jugal and quadratojugal in early birds and their dinosaurian relatives. The Anatomical Record 300:62–75.

Wilberg EW. 2015. What's in an outgroup? The impact of outgroup choice on the phylogenetic position of Thalattosuchia (Crocodylomorpha) and the origin of Crocodyliformes. Systematic Biology 64:621–37.

Wilberg EW, Turner AH, Brochu CA. 2019. Evolutionary structure and timing of major habitat shifts in Crocodylomorpha. Scientific Reports 9.

Willis RE, McAliley LR, Neeley ED, Densmore LD. 2007. Evidence for placing the false gharial (*Tomistoma schlegelii*) into the family Gavialidae: Inferences from nuclear gene sequences. Molecular Phylogenetics and Evolution 43:787–94.

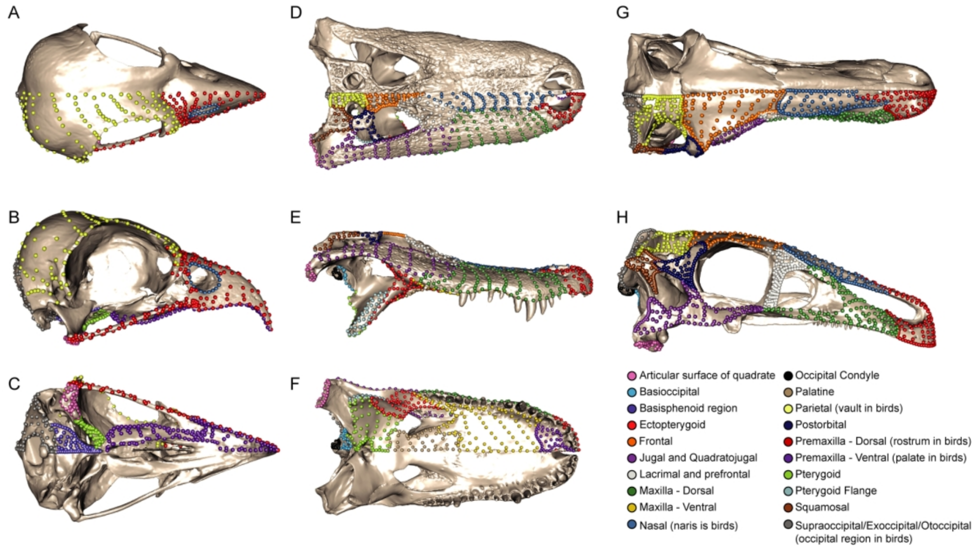

Figure 1: Cranial regions in birds (dorsal, A; lateral, B; ventral, C), mesoeucrocodylians (dorsal, D; lateral, E; ventral, F), and non-avian dinosaurs (dorsal, G; lateral, H) characterized in this study. Three-dimensional surface semilandmarks were placed on digital skull models using the “Morpho” R package (Schlager 2017). Colors of landmarks indicate the cranial region based on the most parameterized model of modularity for that group. Landmarks are illustrated on Pandion haliaetus (USNM 623422, A-C) Alligator mississippiensis (AMNH R-40582, D-F) and Erlikosaurus andrewsi (IGM 100/111, G-H).

162x93mm (300 x 300 DPI)

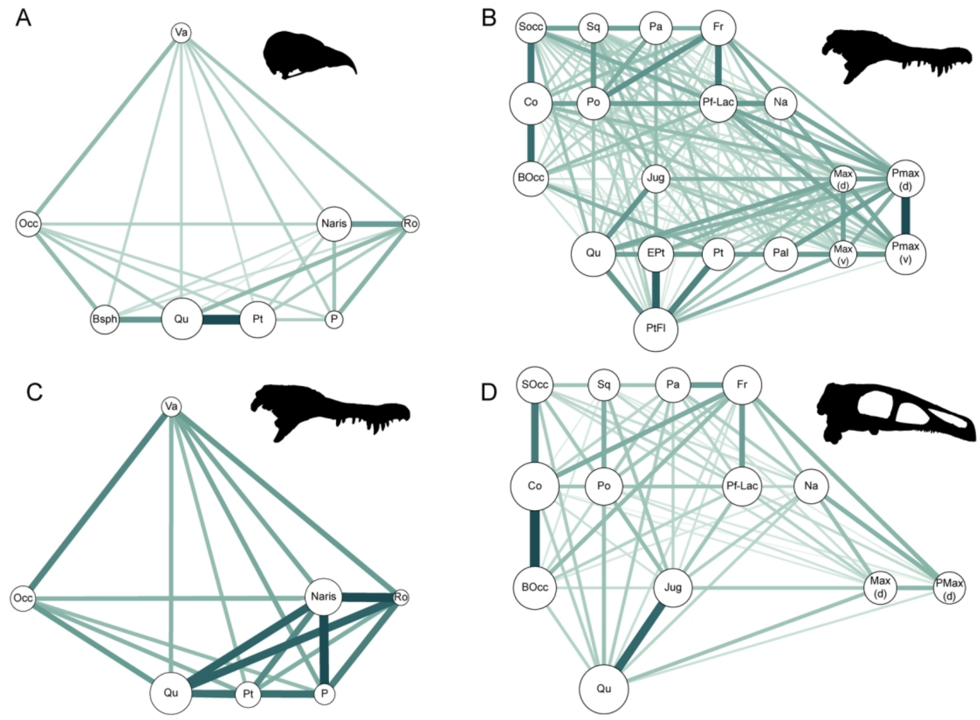

Figure 2: Networks diagrams illustrating the results of phylogenetically-informed EMMLi analyses. Nodes represent cranial regions, with the size of the circle scaled to the magnitude of within-region correlation. Lines connecting nodes represent the strength of correlation between regions, with darker, thicker lines representing higher correlation. Network plots are illustrated for birds (A), mesoeucrocodylians (B), mesoeucrocodylians with landmarks partitioned according to the regions present in birds (C), and non-avian dinosaurs (D). BOcc: basioccipital, Bsph: basisphenoid region, Co: occipital condyle, Ept: ectopterygoid, Fr: frontal, Jug: jugal and quadratojugal, Pf-Lac: lacrimal and prefrontal, Max(d): dorsolateral side of the maxilla, Max(v): ventral surface of maxilla, Na: nasal, Occ: occipital region, Pa: Parietal, Pal: palatine, P: palate region, PMax(d): dorsolateral side of the premaxilla, PMax(v): ventral surface of premaxilla, Po: postorbital, Pt: pterygoid, PtFl: pterygoid flange, Qu: articular surface of the quadrate, Ro: rostrum region, SOcc: superior occipital region including supraoccipital and otoccipital, Sq: squamosal. [COLOR IN ONLINE EDITION ONLY]

146x108mm (300 x 300 DPI)

Group	Species	Collection	Specimen Number	Present in 9-module dataset	Present in 13-module dataset
Ornithischia	*Chasmosaurus belli*	ROM	843	yes	no
Ornithischia	*Diablosaurus eatoni*	UMNH	VP 16699	yes	no
Ornithischia	*Pachycephalosaurus wyomingensi*	TMP	1997-27-0003	yes	no
Ornithischia	*Panoplosaurus mirus*	ROM	1215	yes	yes
Ornithischia	*Pawpawsaurus campbelli*	SMU	73203	yes	yes
Ornithischia	*Pinacosaurus grangeri*	ZPAL	MgD-II_1	yes	no
Ornithischia	*Prenocephale prenes*	ZPAL	MgD-1/104	yes	yes
Ornithischia	*Protoceratops andrewsi*	AMNH	6433	yes	yes
Ornithischia	*Psittacosaurus mongolensis*	AMNH	6254	yes	yes
Ornithischia	*Stegoceras validum*	UALVP	2	yes	yes
Ornithischia	*Stegosaurus stenops*	NHMUK	PV-R36730	yes	yes
Ornithischia	*Thescelosaurus neglectus*	NCSM	15728	yes	yes
Ornithischia	*Triceratops prorsus*	YPM	1822	yes	no
Sauropodomorpha	*Camarasaurus lentus*	CM	11338	yes	yes
Sauropodomorpha	*Diplodocus carnegiei*	CM	11161	yes	yes
Sauropodomorpha	*Massospondylus carinatus*	BPI	BP/1/5241	yes	no
Sauropodomorpha	*Plateosaurus engelhardti*	MB	R.1937	yes	yes
Theropoda	*Allosaurus fragilis*	MOR	693	yes	yes
Theropoda	*Carnotaurus sastrei*	TMP	1997-27-0003	yes	no
Theropoda	*Citipati osmolskae*	IGM	100-978	yes	yes
Theropoda	*Erlikosaurus andrewsi*	IGM	100/111	yes	yes
Theropoda	*Garudimimus brevipes*	GIN	100/13	yes	yes
Theropoda	*Incisivosaurus gauthieri*	IVPP	V-13326	yes	no
Theropoda	*Majungasaurus crenatissimus*	FMNH	PR 2100	yes	yes
Theropoda	*Ornithomimus edmontonicus*	TMP	1995.110.0001	yes	yes
Theropoda	*Struthiomimus altus*	TMP	1990.026.0001	yes	yes
Theropoda	*Tyrannosaurus rex*	BHI	3033	yes	yes

Family	Species	Collection	Specimen Number
Struthionidae	Struthio camelus	MNHN	1908160
Rheidae	Rhea americana	MNHN	1878730
Casuariidae	Casuarius bennetti	NHMUK	1950231
Casuariidae	Casuarius unappendiculatus	USNM	489302
Dromaiidae	Dromaius novaehollandiae	USNM	500379
Apterygidae	Apteryx australis	YPM	110849
Tinamidae	Crypturellus cinereus	USNM	428833
Tinamidae	Rhynchotus rufescens	NHMUK	S-1952-1-24
Tinamidae	Nothoprocta ornata	USNM	620751
Tinamidae	Eudromia elegans	USNM	345094
Cracidae	Ortalis motmot	USNM	621705
Cracidae	Penelope purpurascens	USNM	288719
Cracidae	Crax rubra	NHMUK	18537127
Megapodiidae	Alectura lathami	MNHN	18811115
Phasianidae	Perdix perdix	USNM	553824
Phasianidae	Coturnix coturnix	USNM	603427
Phasianidae	Rollulus rouloul	NHMUK	189172087
Phasianidae	Gallus gallus	MNHN	1880207
Phasianidae	Tetrao urogallus	YPM	102910
Phasianidae	Bonasa umbellus	YPM	1046402
Phasianidae	Meleagris gallopavo	USNM	346978
Numididae	Numida meleagris	USNM	290390
Odontophoridae	Colinus virginianus	NHMUK	S-1994-64-2
Odontophoridae	Odontophorus gujanensis	USNM	621708
Odontophoridae	Odontophorus capueira	MNHN	1868-180
Anhimidae	Chauna chavaria	NHMUK	S-1954-3-3
Anhimidae	Chauna torquata	USNM	347352
Anseranatidae	Anseranas semipalmata	USNM	347638
Anatidae	Dendrocygna arcuata	NHMUK	20122804
Anatidae	Oxyura jamaicensis	NHMUK	S-2004-18-1
Anatidae	Cygnus cygnus	MNHN	1893482
Anatidae	Anser anser	USNM	291065
Anatidae	Branta canadensis	USNM	488182
Anatidae	Anas platyrhynchos	USNM	631964
Anatidae	Aythya valisineria	NHMUK	S-2002471
Turnicidae	Turnix suscitator	USNM	562147
Turnicidae	Turnix velox	AMNH	9658
Indicatoridae	Indicator maculatus	USNM	631581
Indicatoridae	Indicator indicator	USNM	430329
Picidae	Jynx torquilla	USNM	602914
Picidae	Picoides pubescens	USNM	498607
Picidae	Celeus flavescens	AMNH	4212
Picidae	Dryocopus pileatus	FMNH	349048
Picidae	Picus viridis	AMNH	31676
Ramphastidae	Megalaima haemacephala	USNM	613080
Ramphastidae	Capito niger	FMNH	290503
Ramphastidae	Eubucco bourcierii	USNM	560025
Ramphastidae	Semnornis ramphastinus	USNM	346963
Ramphastidae	Aulacorhynchus haematopygus	AMNH	27846
Ramphastidae	Ramphastos sulfuratus	USNM	612339
Galbulidae	Galbula ruficauda	AMNH	25635
Galbulidae	Galbula dea	USNM	623088
Bucconidae	Bucco capensis	USNM	621739
Bucconidae	Chelidoptera tenebrosa	USNM	622945
Bucerotidae	Tockus erythrorhynchus	USNM	322992
Bucerotidae	Buceros rhinoceros	USNM	346727
Bucorvidae	Bucorvus abyssinicus	MNHN	1884-437
Upupidae	Upupa epops	NHMUK	S-1968-4-2
Phoeniculidae	Phoeniculus bollei	AMNH	4232
Trogonidae	Trogon viridis	USNM	561286
Coraciidae	Coracias benghalensis	USNM	343284
Coraciidae	Eurystomus gularis	USNM	292414
Brachypteraciidae	Brachypteracias leptosomus	FMNH	438658
Brachypteraciidae	Atelornis pittoides	FMNH	438663
Momotidae	Baryphthengus martii	USNM	614002
Momotidae	Baryphthengus ruficapillus	USNM	428200
Momotidae	Momotus momota	USNM	344673
Alcedinidae	Alcedo atthis	YPM	102931
Alcedinidae	Todiramphus pyrrhopygius	NHMUK	S-1969-4-432
Alcedinidae	Megaceryle alcyon	USNM	502300
Alcedinidae	Chloroceryle aenea	USNM	623157
Meropidae	Merops viridis	NHMUK	S-1969-1-463
Meropidae	Merops nubicus	USNM	322454
Coliidae	Colius striatus	USNM	558542
Cuculidae	Clamator glandarius	USNM	431797
Cuculidae	Cuculus canorus	USNM	490322
Cuculidae	Cuculus pallidus	NHMUK	1966-50-34
Cuculidae	Coua gigas	FMNH	360040
Cuculidae	Centropus phasianinus	MNHM	A-4173
Cuculidae	Tapera naevia	UMMZ	222,217
Cuculidae	Geococcyx californianus	USNM	610961
Opisthocomidae	Opisthocomus hoazin	YPM	109944
Psittacidae	Probosciger aterrimus	USNM	346724
Psittacidae	Cacatua alba	USNM	557129
Psittacidae	Lorius lory	USNM	557119
Psittacidae	Nestor notabilis	USNM	19876
Psittacidae	Micropsitta bruijnii	AMNH	28102
Psittacidae	Barnardius zonarius	AMNH	29922
Psittacidae	Melopsittacus undulatus	YPM	102222
Psittacidae	Psittacus erithacus	MNHN	1967116
Psittacidae	Anodorhynchus leari	MNHN	1997431
Psittacidae	Amazona guildingii	USNM	613763
Psittacidae	Deroptyus accipitrinus	FMNH	106399
Apodidae	Streptoprocne semicollaris	USNM	489351
Apodidae	Chaetura pelagica	USNM	492655
Apodidae	Apus apus	YPM	1023863
Hemiprocnidae	Hemiprocne mystacea	AMNH	6982
Trochilidae	Phaethornis superciliosus	FMNH	386765
Trochilidae	Eutoxeres condamini	FMNH	291752
Trochilidae	Amazilia tzacatl	USNM	613408
Trochilidae	Archilochus colubris	NHMUK	S-2001.27.4
Musophagidae	Tauraco erythrolophus	AMNH	27414
Musophagidae	Ruwenzorornis johnstoni	FMNH	355262
Musophagidae	Musophaga violacea	FMNH	104075
Musophagidae	Corythaeola cristata	AMNH	247842
Tytonidae	Tyto alba	NHMUK	S-2014-4-71
Strigidae	Bubo bubo	USNM	610383
Strigidae	Strix aluco	NHMUK	S-1975-49-3
Strigidae	Strix nigrolineata	USNM	613976
Strigidae	Athene noctua	USNM	490358
Strigidae	Asio otus	MNHN	1997-457
Aegothelidae	Aegotheles cristatus	USNM	620228
Podargidae	Podargus strigoides	USNM	632131
Steatornithidae	Steatornis caripensis	USNM	560206
Nyctibiidae	Nyctibius grandis	USNM	623085
Nyctibiidae	Nyctibius griseus	USNM	610497
Caprimulgidae	Eurostopodus macrotis	USNM	431310
Caprimulgidae	Chordeiles minor	YPM	1092372
Caprimulgidae	Caprimulgus carolinensis	YPM	144277
Caprimulgidae	Caprimulgus europaeus	USNM	603601
Caprimulgidae	Caprimulgus aegyptius	USNM	641346
Caprimulgidae	Caprimulgus macrurus	USNM	557180
Columbidae	Columba livia	YPM	107622
Columbidae	Columbina passerina	USNM	554675
Columbidae	Leptotila verreauxi	FMNH	104057
Columbidae	Treron curvirostra	MNHN	1884-2475
Columbidae	Ptilinopus roseicapilla	MNHN	1888-34
Eurypygidae	Eurypyga helias	MNHN	1869-396
Otididae	Otis tarda	USNM	289732
Otididae	Ardeotis australis	UMMZ	211,267
Otididae	Chlamydotis undulata	NHMUK	S-2010-5-2
Gruidae	Balearica pavonina	MNHM	1906-75
Gruidae	Balearica regulorum	USNM	637581
Gruidae	Grus antigone	NHMUK	S-1952-2-149
Gruidae	Grus virgo	MNHM	1877-660
Gruidae	Grus americana	USNM	623326
Aramidae	Aramus guarauna	USNM	635727
Psophiidae	Psophia crepitans	MNHN	2013-314
Cariamidae	Cariama cristata	NHMUK	1853-7-12-8
Cariamidae	Chunga burmeisteri	FMNH	106731
Rallidae	Micropygia schomburgkii	USNM	639367
Rallidae	Porzana atra	USNM	562787
Rallidae	Porphyrio porphyrio	MNHN	1909-511
Rallidae	Gallinula chloropus	NHMUK	S-1981-13-35
Mesitornithidae	Monias benschi	USNM	290927
Pteroclididae	Pterocles gutturalis	USNM	430847
Thinocoridae	Thinocorus orbignyianus	USNM	637907
Scolopacidae	Limosa lapponica	MNHN	1997-414
Scolopacidae	Numenius arquata	NHMUK	S-1977-21-1
Scolopacidae	Tringa totanus	YPM	115142
Rostratulidae	Rostratula benghalensis	USNM	613017
Rostratulidae	Rostratula semicollaris	USNM	612032
Jacanidae	Jacana spinosa	USNM	554280
Chionidae	Chionis albus	NHMUK	S-1973-66-85
Chionidae	Pluvianellus socialis	AMNH	17700
Burhinidae	Burhinus oedicnemus	MNHN	1877-333
Burhinidae	Burhinus bistriatus	USNM	621089
Haematopodidae	Haematopus ostralegus	MNHN	ME-3752
Recurvirostridae	Himantopus himantopus	MNHN	1880-271
Recurvirostridae	Himantopus mexicanus	USNM	635762
Recurvirostridae	Recurvirostra avosetta	NHMUK	1954-26-1
Charadriidae	Pluvialis squatarola	YPM	108400
Charadriidae	Charadrius vociferus	USNM	553645
Charadriidae	Vanellus vanellus	MNHN	1931-1953
Dromadidae	Dromas ardeola	NHMUK	S-1957-7-11
Glareolidae	Pluvianus aegyptius	AMNH	24771
Glareolidae	Rhinoptilus africanus	USNM	431520
Glareolidae	Cursorius cursor	USNM	603507
Stercorariidae	Stercorarius parasiticus	USNM	502330
Laridae	Larus marinus	CM	5075
Laridae	Larus philadelphia	YPM	103857
Laridae	Sterna hirundo	NHMUK	S-1975-65-3
Laridae	Chlidonias niger	USNM	499661
Alcidae	Uria aalge	YPM	111991
Alcidae	Cepphus grylle	USNM	612213
Alcidae	Fratercula arctica	MNHN	1888-339
Accipitridae	Pandion haliaetus	USNM	623422
Accipitridae	Pernis apivorus	MNHN	1997-309
Accipitridae	Gampsonyx swainsonii	USNM	622231
Accipitridae	Haliaeetus albicilla	USNM	292774
Accipitridae	Haliaeetus leucocephalus	MNHN	A-4056
Accipitridae	Neophron percnopterus	USNM	17835
Accipitridae	Gyps fulvus	MNHN	1995-160
Accipitridae	Aegypius monachus	AMNH	1939
Accipitridae	Accipiter nisus	USNM	344423
Accipitridae	Buteo buteo	NHMUK	S-1972-11-59
Accipitridae	Aquila chrysaetos	MNHN	1930-152
Accipitridae	Sagittarius serpentarius	AMNH	1306
Falconidae	Micrastur semitorquatus	USNM	245788
Falconidae	Ibycter americanus	YPM	139300
Falconidae	Phalcoboenus australis	USNM	490979
Falconidae	Falco peregrinus	USNM	491265
Podicipedidae	Podiceps cristatus	USNM	560594
Phaethontidae	Phaethon aethereus	USNM	18555
Phaethontidae	Phaethon lepturus	NHMUK	1898-91-676
Sulidae	Morus bassanus	MNHN	199018
Sulidae	Sula dactylatra	NHMUK	S-1975-3-71
Anhingidae	Anhinga anhinga	CM	26
Phalacrocoracidae	Phalacrocorax carbo	USNM	18851
Ardeidae	Tigrisoma lineatum	USNM	631043
Ardeidae	Ixobrychus minutus	USNM	603399
Ardeidae	Nycticorax nycticorax	USNM	501635
Ardeidae	Egretta garzetta	USNM	430820
Ardeidae	Ardea purpurea	MNHN	1997-225
Ardeidae	Casmerodius albus	USNM	610600
Ardeidae	Bubulcus ibis	MNHN	1997-208
Scopidae	Scopus umbretta	NHMUK	1897-5-10-38
Phoenicopteridae	Phoenicopterus ruber	MNHN	1882-2064
Threskiornithidae	Eudocimus ruber	USNM	322060
Threskiornithidae	Theristicus caerulescens	USNM	635755
Threskiornithidae	Mesembrinibis cayennensis	USNM	562523
Threskiornithidae	Threskiornis aethiopicus	USNM	558414
Threskiornithidae	Platalea leucorodia	MNHN	ME48
Threskiornithidae	Platalea ajaja	MNHN	1884-2571
Balaenicipitidae	Balaeniceps rex	USNM	344963
Pelecanidae	Pelecanus occidentalis	USNM	489428
Cathartidae	Cathartes aura	USNM	17872
Cathartidae	Vultur gryphus	NHMUK	S-1956-1-81
Cathartidae	Sarcoramphus papa	MNHN	A4002-IV/188
Ciconiidae	Ciconia maguari	NHMUK	S-1955-5-2
Ciconiidae	Ciconia ciconia	MNHN	187979
Ciconiidae	Leptoptilos dubius	USNM	225988
Fregatidae	Fregata magnificens	USNM	610592
Fregatidae	Fregata minor	MNHN	1997-180
Spheniscidae	Aptenodytes forsteri	UMMZ	216,161
Spheniscidae	Pygoscelis adeliae	NHMUK	S-1966-42
Spheniscidae	Spheniscus humboldti	MNHN	1965-162
Gaviidae	Gavia stellata	USNM	561404
Procellariidae	Fulmarus glacialis	NHMUK	1898-71-21
Procellariidae	Lugensa brevirostris	MNHN	2004-378
Procellariidae	Pterodroma macroptera	USNM	500654
Procellariidae	Calonectris diomedea	MNHN	2004-413
Procellariidae	Puffinus puffinus	MNHN	1997-170
Pelecanoididae	Pelecanoides georgicus	AMNH	3232
Pelecanoididae	Pelecanoides urinatrix	NHMUK	S-1916-1-21
Diomedeidae	Diomedea exulans	NHMUK	1848-8-31-36
Diomedeidae	Phoebastria nigripes	USNM	630953
Diomedeidae	Thalassarche chlororhynchos	YPM	102976
Hydrobatidae	Pelagodroma marina	USNM	614205
Hydrobatidae	Oceanodroma tethys	USNM	614199
Acanthisittidae	Xenicus gilviventris	NHMUK	S-1972-1-108
Pittidae	Pitta sordida	USNM	432055
Eurylaimidae	Smithornis capensis	FMNH	444067
Eurylaimidae	Eurylaimus ochromalus	YPM	104081
Eurylaimidae	Calyptomena viridis	UMMZ	2,180,902
Philepittidae	Philepitta castanea	FMNH	393177
Tyrannidae	Rhynchocyclus brevirostris	YPM	1445212
Tyrannidae	Hymenops perspicillatus	YPM	1011092
Tyrannidae	Tyrannus savana	USNM	635850
Tyrannidae	Tyrannus tyrannus	AMNH	31397
Cotingidae	Pachyramphus minor	NHMUK	1891.7.20.308
Cotingidae	Cephalopterus ornatus	FMNH	106996
Cotingidae	Rupicola peruvianus	YPM	109149
Pipridae	Pipra rubrocapilla	YPM	1057413
Thamnophilidae	Sakesphorus luctuosus	USNM	562278
Furnariidae	Furnarius rufus	YPM	1032362
Dendrocolaptidae	Campylorhamphus trochilirostris	FMNH	321456
Formicariidae	Formicarius analis	USNM	614119
Formicariidae	Formicarius rufipectus	USNM	559999
Formicariidae	Grallaria ruficapilla	AMNH	24122
Conopophagidae	Conopophaga ardesiaca	FMNH	322380
Rhinocryptidae	Scytalopus magellanicus	AMNH	24350
Climacteridae	Climacteris rufus	AMNH	29997
Menuridae	Menura novaehollandiae	USNM	632118
Ptilonorhynchidae	Sericulus chrysocephalus	FMNH	106327
Ptilonorhynchidae	Ptilonorhynchus violaceus	USNM	428269
Meliphagidae	Meliphaga lewinii	MNHN	ZO-AC-1873-480
Pardalotidae	Pardalotus striatus	NHMUK	S-1966-51-192
Petroicidae	Drymodes brunneopygia	AMNH	29949
Irenidae	Irena puella	FMNH	104162
Chloropseidae	Chloropsis aurifrons	FMNH	1042982
Laniidae	Lanius ludovicianus	USNM	554039
Vireonidae	Vireo olivaceus	AMNH	31488
Corcoracidae	Struthidea cinerea	USNM	224841
Pachycephalidae	Pachycephala philippinensis	FMNH	392304
Colluricinclidae	Colluricincla harmonica	NHMUK	S-1966-51-171
Corvidae	Garrulus glandarius	MNHN	1931-254
Corvidae	Corvus brachyrhynchos	USNM	553267
Corvidae	Corvus corone	NHMUK	S-1976-271
Cnemophilidae	Cnemophilus loriae	YPM	105212
Paradisaeidae	Lophorina superba	CM	4964
Paradisaeidae	Paradisaea minor	FMNH	104462
Paradisaeidae	Paradisaea raggiana	USNM	500630
Paradisaeidae	Paradisaea rudolphi	USNM	321104
Cracticidae	Gymnorhina tibicen	USNM	632142
Oriolidae	Oriolus oriolus	FMNH	369196
Campephagidae	Coracina novaehollandiae	CM	S-15217
Rhipiduridae	Rhipidura albicollis	NHMUK	S-1969-1-179
Dicruridae	Dicrurus macrocercus	USNM	292203
Dicruridae	Dicrurus megarhynchus	USNM	6150582
Monarchidae	Myiagra hebetior	USNM	615036
Vangidae	Vanga curvirostris	spec	†2017-254
Dulidae	Dulus dominicus	AMNH	25478
Bombycillidae	Phainopepla nitens	YPM	1076902
Bombycillidae	Bombycilla garrulus	YPM	1122922
Bombycillidae	Bombycilla cedrorum	YPM	109267
Cinclidae	Cinclus mexicanus	FMNH	288098
Turdidae	Catharus fuscescens	USNM	501951
Turdidae	Turdus merula	NHMUK	S-1975-29-1
Turdidae	Turdus philomelos	MNHN	1997-663
Muscicapidae	Culicicapa ceylonensis	YPM	107307
Muscicapidae	Cichladusa guttata	FMNH	369058
Muscicapidae	Oenanthe oenanthe	AMNH	17960
Sturnidae	Sturnus unicolor	YPM	1050553
Sturnidae	Leucopsar rothschildi	USNM	553653
Sturnidae	Buphagus erythrorhynchus	USNM	491371
Mimidae	Toxostoma redivivum	USNM	636895
Sittidae	Sitta europaea	NHMUK	S-1952-2-669
Mimidae	Donacobius atricapilla	UMMZ	227,534
Troglodytidae	Thryothorus ludovicianus	YPM	1082373
Paridae	Parus atricapillus	YPM	103511
Hirundinidae	Hirundo rustica	YPM	1044832
Reguliidae	Regulus satrapa	NHMUK	S-1998-103-25
Sylviidae	Bernieria zosterops	YPM	1035122
Pycnonotidae	Nicator chloris	AMNH	24864
Cisticolidae	Cisticola cantans	FMNH	313190
Sylviidae	Locustella naevia	NHMUK	S-1981-66-1
Sylviidae	Acrocephalus arundinaceus	YPM	1012652
Sylviidae	Sylvietta leucophrys	FMNH	346504
Sylviidae	Hylia prasina	AMNH	19071
Sylviidae	Phylloscopus ruficapilla	FMNH	3567873
Timaliidae	Garrulax galbanus	CM	S-16131
Timaliidae	Illadopsis cleaveri	NHMUK	S-1911-5-31-357
Timaliidae	Stachyris whiteheadi	FMNH	3877432
Timaliidae	Rhopocichla atriceps	FMNH	355736
Timaliidae	Leiothrix lutea	TPM	1032712
Timaliidae	Yuhina brunneiceps	YPM	1073812
Sylviidae	Oxylabes madagascariensis	FMNH	384714
Alaudidae	Calandrella rufescens	NHMUK	S-1952-2-601
Dicaeidae	Dicaeum ignipectus	USNM	3923153
Melanocharitidae	Melanocharis versteri	YPM	106461
Passeridae	Passer domesticus	USNM	604859
Motacillidae	Motacilla alba	FMNH	106864
Prunellidae	Prunella modularis	NHMUK	S-1973-25-1
Ploceidae	Ploceus nigricollis	AMNH	17116
Estrildidae	Taeniopygia guttata	YPM	1028203
Viduidae	Vidua macroura	FMNH	313258
Fringillidae	Bucanetes githagineus	MNHN	1997-561
Fringillidae	Loxia leucoptera	USNM	622723
Emberizidae	Emberiza cirlus	MNHN	1997-753
Emberizidae	Calcarius lapponicus	NHMUK	S-1958-20-1
Emberizidae	Plectrophenax nivalis	FMNH	4289682
Emberizidae	Spizella passerina	NHMUK	S-1955-1-48
Emberizidae	Pipilo chlorurus	AMNH	21692
Parulidae	Dendroica petechia	NHMUK	S-1986-60-66
Thraupidae	Tangara schrankii	CM	S-153202
Emberizidae	Geospiza fortis	USNM	345593
Emberizidae	Geospiza fuliginosa	USNM	345595
Cardinalidae	Cardinalis cardinalis	AMNH	26587
Cardinalidae	Saltator albicollis	AMNH	7249
Icteridae	Psarocolius wagleri	UMMZ	209,355
Icteridae	Quiscalus mexicanus	YPM	107757

Family	Species	Collection	Specimen Number	Fossil?
Alligatoridae	*Alligator mississippiensis*	AMNH	R-40582	no
Alligatoridae	*Alligator sinensis*	AMNH	R-23900	no
Alligatoridae	*Caiman crocodilus*	MCZ	5031	no
Alligatoridae	*Caiman latirostris*	NHMUK	2009.1	no
Alligatoridae	*Caiman yacare*	AMNH	97299	no
Alligatoridae	*Leidyosuchus canadensis*	TMP	74-10-08	yes
Alligatoridae	*Melanosuchus niger*	AMNH	58132	no
Alligatoridae	*Osteolaemus tetraspis*	MCZ	17704	no
Alligatoridae	*Paleosuchus palpebrosus*	ZSM	41-1938	no
Alligatoridae	*Paleosuchus trigonatus*	AMNH	6691	no
Alligatoridae	*Procaimanoidea utahensis*	USNM	V-15996	yes
Alligatoridae	*Purussaurus neivensis*	UCMP	39704	yes
Crocodylidae	*Crocodylus acutus*	MNHN	A-5310	no
Crocodylidae	*Crocodylus affinus*	UWBM	88113	yes
Crocodylidae	*Crocodylus intermedius*	MNHN	1885-489	no
Crocodylidae	*Crocodylus johnstoni*	TMM	M-6807	no
Crocodylidae	*Crocodylus mindorensis*	FMNH	11136-7	no
Crocodylidae	*Crocodylus moreletii*	MNHN	21012	no
Crocodylidae	*Crocodylus niloticus*	USNM	64011	no
Crocodylidae	*Crocodylus novaeguineae*	AMNH	64425	no
Crocodylidae	*Crocodylus palustris*	MNHN	1941-210	no
Crocodylidae	*Crocodylus porosus*	USNM	210131	no
Crocodylidae	*Crocodylus raninus*	AMNH	29294	no
Crocodylidae	*Crocodylus rhombifer*	MCZ	4042	no
Crocodylidae	*Crocodylus siamensis*	NHMUK	1920.1.20	no
Crocodylidae	*Mecistops cataphractus*	AMNH	10075	no
Crocodylidae	*Prodiplocynodon langi*	AMNH	108	yes
Crocodylidae	*Voay robustus*	AMNH	3101	yes
Gavialidae	*Gavialis gangeticus*	UF	118998	no
?Gavialidae	*Tomistoma schlegelii*	MCZ	12459	no
Globidonta	*Stangerochampsa mccabei*	TMP	1986-061-001	yes
Notosuchidae	*Araripesuchus gomesii*	AMNH	24450	yes
Notosuchidae	*Araripesuchus wegeneri*	MNN	GAD19	yes
Notosuchidae	*Kaprosuchus saharicus*	MNN	IGU12	yes
Notosuchidae	*Mariliasuchus amarali*	MZSP	PV 50	yes
Notosuchidae	*Simosuchus clarki*	UA	8679	yes
Pholidosauridae	*Sarcosuchus imperator*	TMP	2009-003-0005	yes
Pristichampsidae	*Pristichampsus vorax*	FMNH	PR-399	yes

Abbreviation	Institution	Location
AMNH	American Museum of Natural History	New York
CM	Carnegie Museum	Pittsburgh
FMNH	Field Museum	Chicago
MNHN	Muséum National díHistoire Naturelle	Paris
USNM	National Museum of Natural History	Washington DC
UMMZ	University of Michigan Museum of Zoology,	Ann Arbor
YPM	Yale Peabody Museum	New Haven
TMP	Royal Tyrell Museum	Drumheller
NHMUK	Museum of Natural History	London
MOR	Museum of the Rockies	Bozeman
ROM	Royal Ontario Museum	Toronto
IGM	Mongolian Academy of Sciences	Ulaanbaatar
UMNH	Natural History Museum of Utah	Salt Lake City
GIN	Mongolian Academy of Sciences	Ulaanbaatar
IVPP	Institute of Vertebrate Paleontology and Paleoanthropology	Beijing
BPI	Evolutionary Studies Institute, University of the Witwatersrand	Johannesburg
SMU	Schuler Museum of Paleontology, Southern Methodist University	Dallas
ZPAL	Institute of Paleobiology, Polish Academy of Sciences	Warsaw
MB	Museum für Naturkunde Berlin	Berlin
UALVP	University of Alberta Laboratory for Vertebrate Paleontology	Edmonton
NCSM	North Carolina Museum of Natural Sciences	Raliegh
BHI	Black Hills Institute	Hill City
MNN	Musee National du Niger	Niamey
MCZ	Museum of Comparative Zoology	Cambridge, MA
UWBM	Burke Museum of Natural History	Seattle
TMM	Texas Memorial Museum	Austin
UF	Florida Museum of Natural History	Gainesville
MZSP	Museu de Zoologia da Universidade de São Paulo	São Paulo
ZSM	Bavarian State Collection of Zoology	Munich
UCMP	University of California Museum of Paleontology	Berkeley
UA	Universite´ d'Antananarivo	Antananarivo

Electronic Supplemental Material 2:
Landmark Definitions for Mesoeucrocodylians and Non-avian Dinosaur Datasets

Bird specimens were landmarked following Felice and Goswami (2018)

Table S2A: Landmark Definitions: Mesoeucrocodylians

Number	Left side counterpart	Description
1	NA	Anterior midline point on premaxilla, ventral side
2	NA	Posterior midline point on premaxilla, ventral side
3	59	Lateral most point on the maxilla-premaxilla suture, ventral side
4	NA	Posterior midline point on maxilla, ventral side
5	60	Posterolateral most point on maxilla, ventral side
6	61	Lateral most point on the maxilla-premaxilla suture, dorsal side
7	NA	Anterior midline point on premaxilla, anterodorsal side
8	NA	Posterior midline on the premaxilla anterior to the naris
9	62	Medial most point on the maxilla-premaxilla suture, dorsal side
10	NA	Anterior midline point on nasal
11	NA	Posterior midline point on nasal
12	63	Posterolateral corner of nasal
13	NA	Posterior midline point on frontal
14	NA	Posterior midline point on parietal
15	64	Posterolateral corner of frontal at the contact with the postorbital
16	65	Anterolateral corner of frontal at the contact with the prefrontal
17	66	Posterolateral corner of parietal at the contact with the squamosal
18	67	Anterolateral corner of frontal at the contact with the frontal
18	NA	Dorsal midline of supraoccipital
20	NA	Dorsal midline of foramen magnum
21	NA	Dorsal midline point on occipital condyle
22	68	Medial point on the otoccipital contact with occipital condyle
23	NA	Ventral midline point on occipital
24	69	Lateral most point on otoccipital
25	NA	Ventral midline basioccipital
26	70	Dorsolateral post point on basioccipital
27	71	Posterolateral point on pterygoid at contact with basioccipital
28	NA	Posterior midline point on pterygoid
29	NA	Anterior midline point on ptergoid
30	72	Posterolateral corner on the ventral surface of the pterygoid
31	73	Anterolateral corner on the ventral surface of the pterygoid
32	NA	Anterior midline point on the palatine
33	74	Posterolateral point on ventral surface of palatine
34	75	Posterior lateral contact between palatine and maxilla
35	76	Medial point on articular surface of quadrate
36	77	lateral point on articular surface of quadrate
37	78	Anterolateral corner of orbit, jugal-lacrimal contact
38	79	Anterior most point on the jugal
39	80	Posterolateral most point on the quadratojugal
40	81	Anterodorsal tip of quadratojugal
41	82	On the jugal, the anterior contact with the post orbital
42	83	Posterolateral point on squamosal
43	84	Anterolateral point on the squamosal (contact with postorbital)
44	85	Posteromedial point on the squamosal (contact with parietal)
45	86	Posterolateral point on the lacrimal
46	87	Anterior most point on the lacrimal
47	88	Medial most point on the prefrontal/lacrimal region
48	89	Posterolateral point on the prefrontal
49	90	Anteromedial corner of squamosal
50	91	Anteromedial point on ectopterygoid
51	92	Posteromedial point on ectopterygoid
52	93	Anterolateral point on ectopterygoid
53	94	Posterolateral point on ectopterygoid
54	95	Dorsal point on pterygoid flange
55	96	Ventral point on pterygoid flange
56	NA	Anterior most point on midline of frontal
57	97	Posterior medial point on palatine
58	98	Anteroventral corner of postorbital

Table S2B: Curve definitions: Mesoeucrocodylians

Curve Number	Description	Number of Semilandmarks
1	Ventral midline of premaxilla	10
2	Ventral maxilla/premaxilla suture	10
3	Lateral border of ventral surface of premaxilla, medial to the teeth	10
4	Ventral midline of the maxilla	10
5	Posteromedial margin of ventral surface of maxilla	20
6	Lateral border of ventral surface of maxilla, medial to the teeth	20
7	Lateral margin of maxilla	20
8	Dorsolateral premaxilla/maxilla suture	10
9	Medial border of the maxilla	10
10	Lateral margin of premaxilla	10
11	Midline of the maxilla anterior to the naris	10
12	Medial margin of premaxilla	10
13	Midline of nasal	10
14	Posterior margin of nasal	5
15	Lateral margin of nasal	10
16	Midline of frontal	10
17	Posterior margin of frontal	10
18	Lateral margin of frontal	10
19	Anterior margin of frontal	10
20	Midline of parietal	5
21	Anterior margin of parietal	10
22	Posterior margin of parietal	10
23	Lateral margin of parietal	10
24	Midline of supraoccipital	10
25	Lateral side of foramen magnum	10
26	Ventrolateral margin of otoccipital	10
27	Dorsal margin of otoccipital and supraoccipital	5
28	Dorsal margin of occipital condyle	10
29	Lateral margin of occipital condyle	5
30	Midline of occipital condyle	10
31	Ventral margin of basioccipital	5
32	Midline of basioccipital	10
33	Midline of pterygoid	5
34	Anterior margin of pterygoid	10
35	Lateral margin of ventral surface of pterygoid	10
36	Posterior margin of pterygoid	10
37	Midline of palatine	10
38	Anterior margin of palatine	10
39	Lateral margin of palatine	5
40	Posterior margin of palatine	10
41	Ventral margin of the orbit on the jugal	5
42	Jugal-lacrimal suture	20
43	Ventral margin of jugal and quadratojugal	10
44	Posterior margin of quadratojugal	10
45	Anterior margin of quadratojugal	10
46	Lateral margin of squamosal	5
47	Anterior margin of squamosal	10
48	Medial margin of squamosal	5
49	Posterior margin of squamosal	10
50	Lateral margin of lacrimal	5
51	Anteromedial margin of lacrimal	10
52	Medial margin of lacrimal and prefrontal	10
53	Anterior margin of orbit, on the prefrontal and lacrimal	10
54	Anterior margin of ectopterygoid	10
55	Medial margin of ectopterygoid	10
56	Posterior margin of ectopterygoid	10
57	Lateral margin of pterygoid	10
58	Posterior margin of pterygoid flange	10
59	Medial margin of ectopterygoid	10
60	Posterior margin of ectopterygoid	10
61	Lateral margin of pterygoid	10
62	Posterior margin of pterygoid flange	10
63	Anterior margin of pterygoid flange	5
64	Posterior margin of articular surface of quadrate	10
65	Anterior margin of articular surface of quadrate	10
66	Posterodorsal margin of the postorbital	5
67	Anterordorsal margin of the postorbital	5
68	Anterior margin of postorbital	10
69	Posterior margin of postorbital	5

Table S2C: Landmark definitions: Non-avian dinosaurs

Number	Left side counterpart	Description
1	48	Posterolateral point on maxilla
2	49	Posterolateral most point on maxilla, ventral side
3	50	Posterolateral most point on the premaxilla
4	NA	Anteromedial most point on the premaxilla (or rostral bone)
5	NA	Posterior midline point on dorsal surface of the maxilla
6	NA	Anterior midline point on nasal
7	51	Anterior most point on medial premaxillary part of the nasal
8	52	Posterodorsal most point on the maxillary part of the premaxilla
9	53	Dorsal most point on the ascending process of the maxilla
10	54	Ventral most point on the descending anterior ramus of the nasal
11	NA	Posterior midline point of the nasal (frontonasal contact)
12	NA	Posterior midline of frontal
13	55	Posterolateral most point on the frontal
14	56	Anterolateral most point on the frontal
15	NA	Posterior midline point on parietal
16	57	Dorsal midline point on supraoccipital
17	58	Dorsal midline of foramen magnum
18	59	Medial point on the exoccipital contact with occipital condyle
19	60	Lateral most point on exoccipital
20	61	Lateral most point of the exoccipital-squamosal suture
21	62	Dorsal midline point on the occipital condyle
22	NA	Ventral midline point on the occipital condyle
23	NA	Lateral contact on exoccipital-basioccipital suture
24	63	Midline point on basioccipital-basisphenoid suture
25	64	Anterolateral most point on the post orbital
26	65	Tip of the descending part of the postorbital
27	66	Posterior most point on the postorbital
28	67	On the jugal, the posterior lacrimal-jugal contact
29	68	Posterior most point on the postorbital process of the jugal
30	69	Anterior contact of the jugal or quadratojugal to maxilla
31	70	Posteroventral most point on the quadratojugal
32	71	Dorsal most point on the posterior part of the quadratojugal
33	72	Ventral most point on the squamosal
34	73	Anterolateral most point on the squamosal
35	74	Anteromedial most point on the squamosal (squamosal-parietal contact)
36	75	Lateral most point on jaw joint
37	76	Medial most point on the jaw joint
38	77	Posterior most point on the jaw joint
39	78	Anterodorsal most point on the jugal
40	79	Posterolateral most point on the prefrontal
41	80	Dorsolateral most point on the lacrimal
42	81	Anterior most point on the ventral extent of the lacrimal
43	82	Posteromedial point on the prefrontal
44	83	Posterolateral point on the nasal
45	84	Parietal fenestra-anterior point
46	85	Parietal fenestra-posteromedial point
47	86	Parietal fenestra-posterolateral point

Table S2D: Semilandmark Curve Definitions: Non-avian Dinosaurs

Curve Number	Description	Number of Semilandmarks
1	Medial margin of the ventral surface of the premaxilla	20
2	Posterior margin of the ventral surface of the premaxilla	20
3	Lateral margin of the ventral surface of the premaxilla	20
4	Medial margin of the ventral surface of the maxilla	20
5	Posterior margin of the ventral surface of the maxilla	20
6	Lateral margin of the ventral surface of the maxilla	20
7	Anterior margin of the ventral surface of the maxilla	20
8	Lateral margin of the maxilla	20
9	Anterior margin of maxilla	20
10	Posterior margin of maxilla	20
11	Lateral margin of premaxilla	20
12	Midline of premaxilla	20
13	Narial margin of the premaxilla	20
14	Premaxilla-maxilla suture	20
15	Midline of nasal	8
16	Posterior margin of the nasal	20
17	Lateral margin of the nasal	20
18	Narial margin of the nasal	8
19	Premaxilla-nasal suture	20
20	Midline of frontal	20
21	Posterior margin of the frontal	20
22	Lateral margin of the frontal	20
23	Anterior margin of the frontal	20
24	Midline of parietal	30
25	Posterior margin of the parietal	20
26	Lateral margin of the parietal	20
27	Anterior margin of the parietal	20
28	Midline of the supraoccipital	15
29	Lateral side of foramen magnum	20
30	Ventral margin of the exoccipital	15
31	Dorsal margin of the exoccipital and supraoccipital	20
32	Lateral margin of the occipital condyle	20
33	Midline of occipital condyle	20
34	Lateral margin of the basioccipital	20
35	Midline of basioccipital	20
36	Posteromedial margin of basisphenoid	20
37	Lateral margin of basisphenoid	20
38	Midline of basisphenoid	20
39	Posteromedial margin of pterygoid	20
40	Lateral margin of pterygoid	20
41	Medial margin of the pterygoid	20
42	Medial margin of palatine	30
43	Posterior margin of pterygoid	20
44	Lateral margin of pterygoid	20
45	Anterior margin of pterygoid	20
46	Anterior margin of postorbital	20
47	Posteroventral margin of postorbital	20
48	Dorsomedial margin of postorbial	20
49	Anterodorsal margin of jugal	20
50	Jugal-maxilla contact	20
51	Ventral margin of jugal and quadratojugal	20
52	Posterior margin of quadratojugal	20
53	Ventral margin of inferior temporal fenestra (on the jugal and quadratojugal)	20
54	Superior margin of jugal	20
55	Anterior margin of squamosal along margin of inferior temporal fenestra	20
56	Anterodorsal margin of squamosal	20
57	Medial margin of the squamosal	15
58	Posterior margin of squamosal	20
59	Posterolateral margin of articular surface of quadrate	20
60	Posteromedial margin of articular surface of quadrate	20
61	Anterior margin of articular surface of quadrate	20
62	Posterior margin of the prefrontal and lacrimal	20
63	Anterior margin of the prefrontal and lacrimal	20
64	Anterolateral margin of parietal fenestra	20
65	Posterior margin of parietal fenestra	20
66	Anteromedial margin of parietal fenestra	20

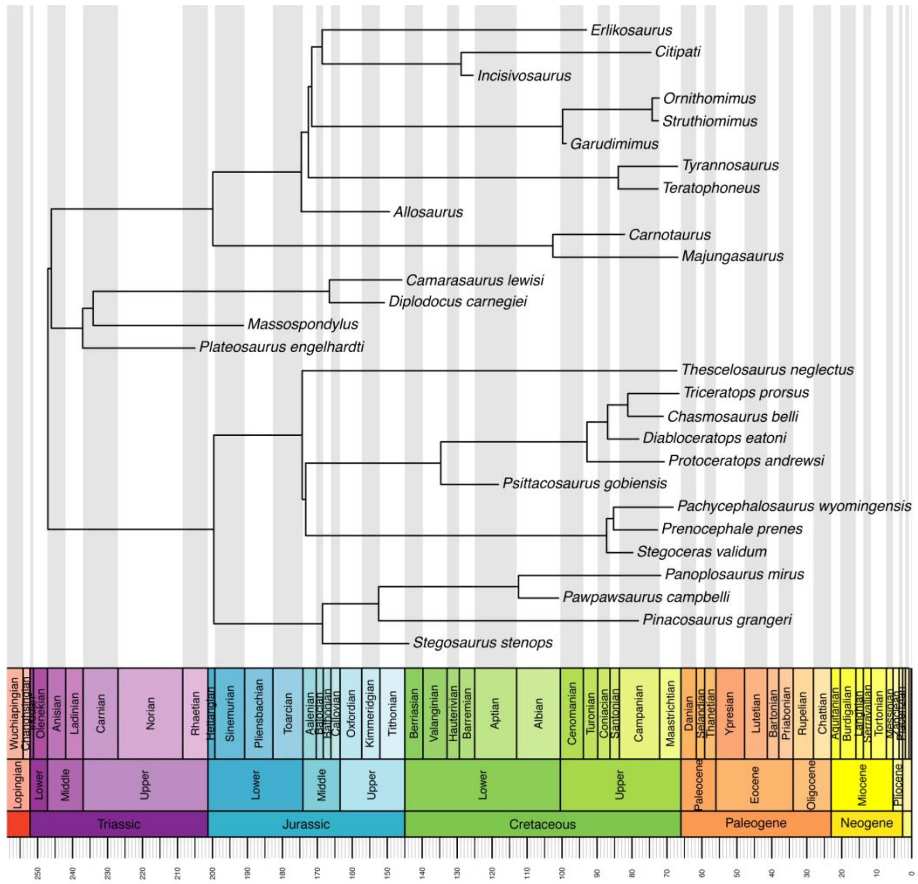

Figure S3A: "Traditional" Dinosaur phylogenetic hypothesis time-scaled using the "paleotree" R package (Bapst 2012)

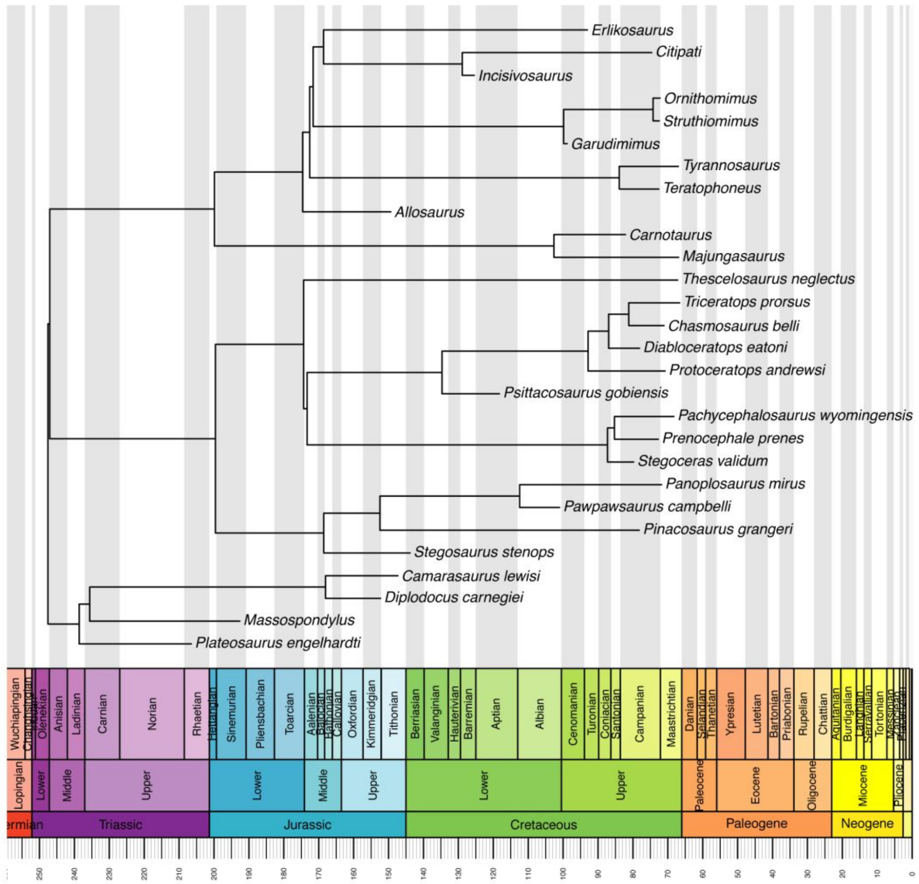

Figure S3B: “Ornithoscelida” dinosaur phylogenetic hypothesis (Baron et al. 2017) time-scaled using the “paleotree” R package (Bapst 2012)

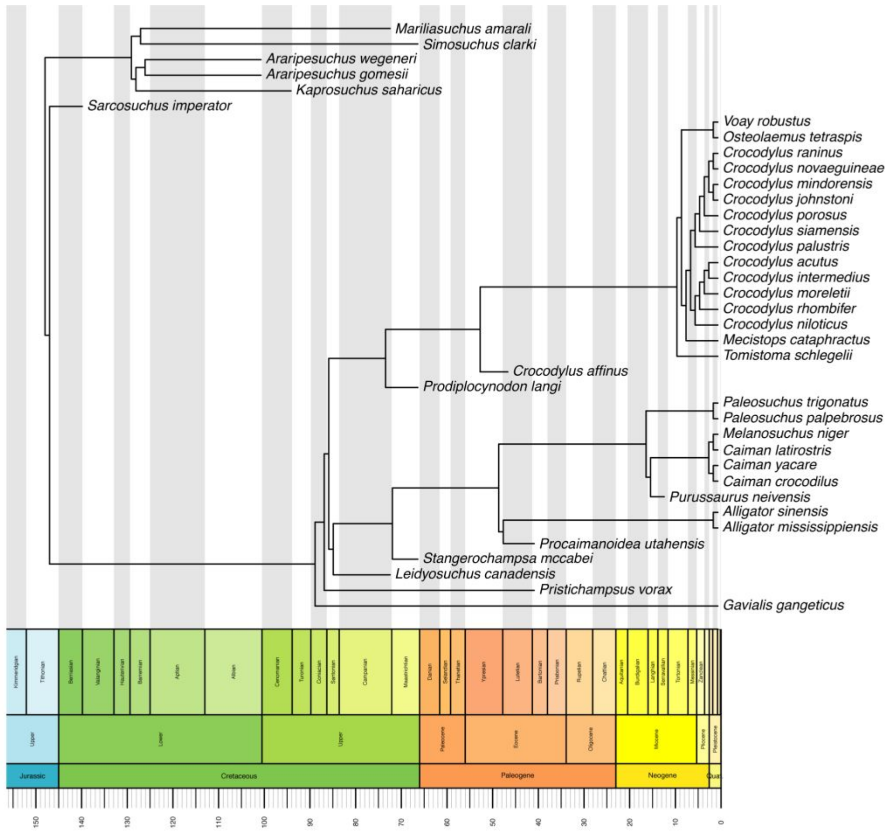

Figure S3C: Crocodylomorph hypothesis "tree 1." Thalattosuchians as neosuchians and *Tomistoma* as Crocodylidae. Time-scaled using the "paleotree" R package (Bapst 2012)

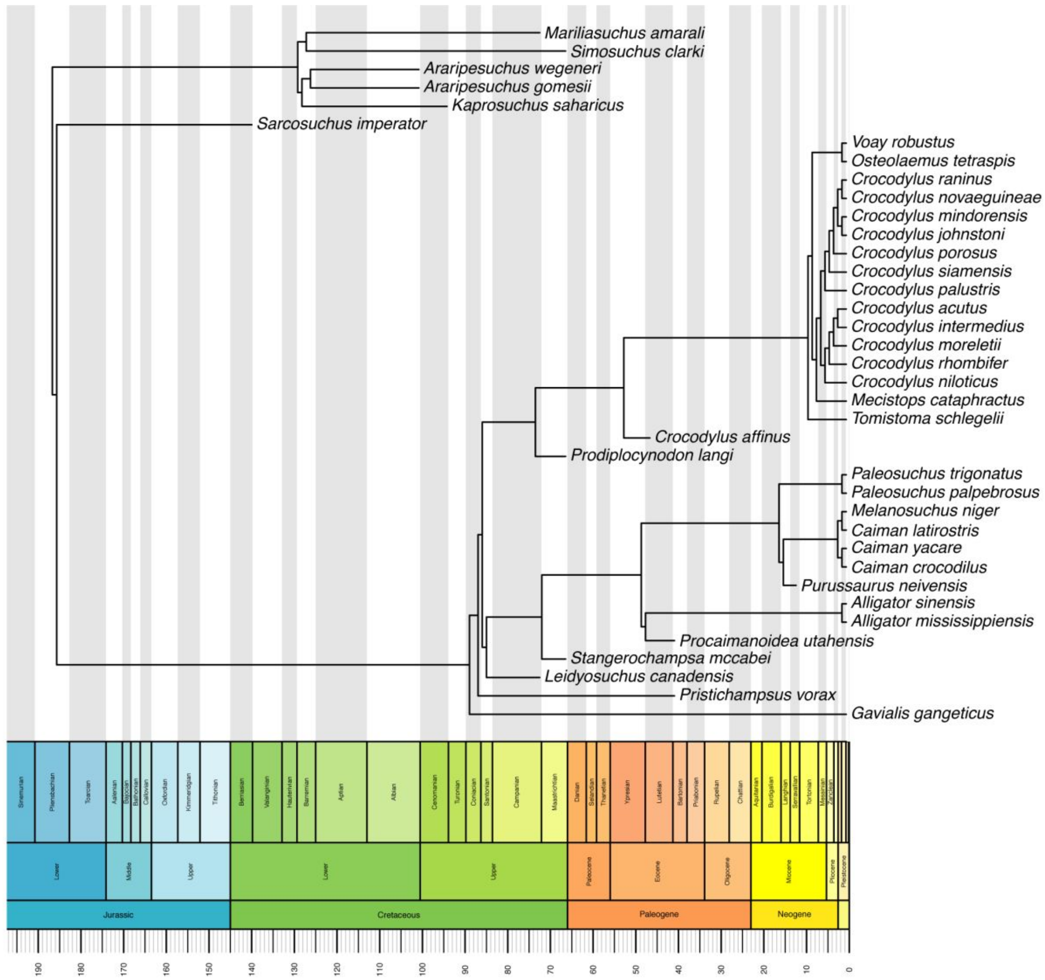

Figure S3C: Crocodylomorph hypothesis "tree 2." Thalattosuchians as basal Crocodyliformes and *Tomistoma* as Crocodylidae
Time-scaled using the "paleotree" R package (Bapst 2012)

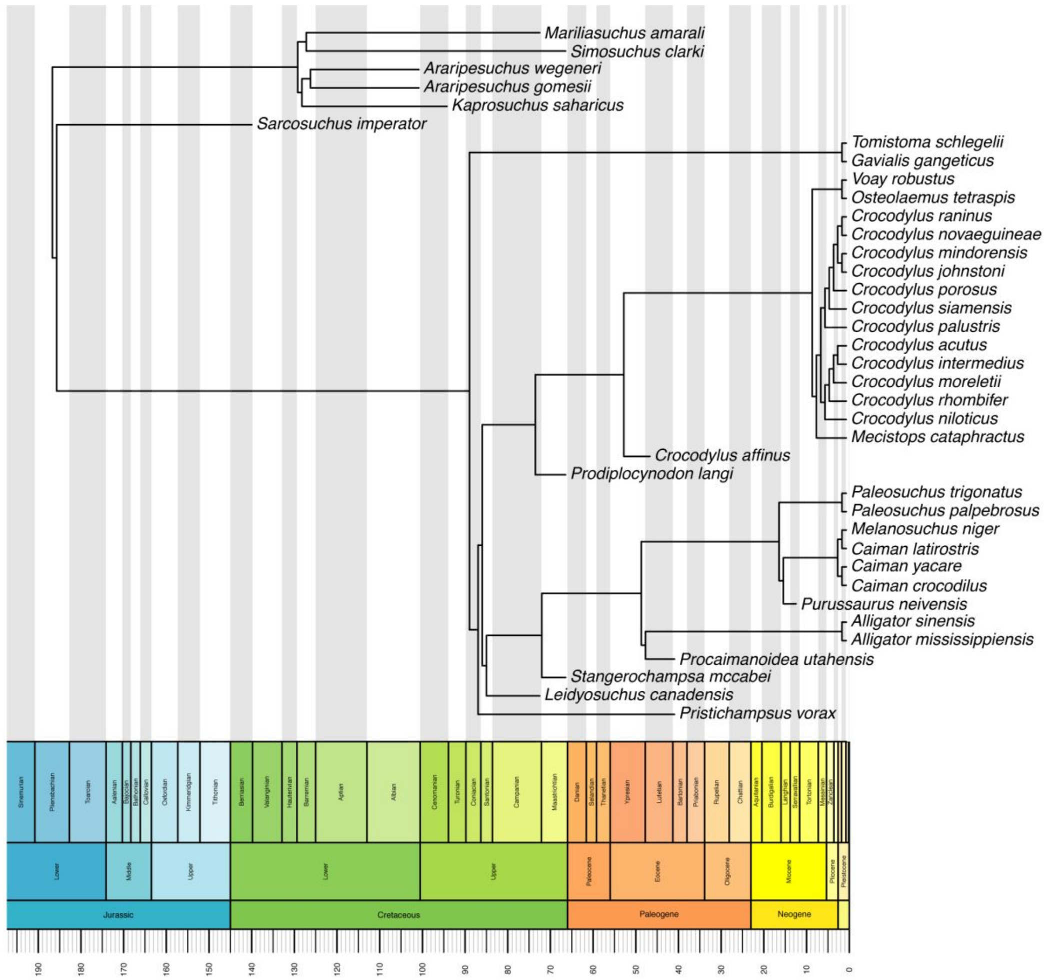

Figure S3E: Crocodylomorph hypothesis “tree 4.” Thalattosuchians as basal Crocodyliformes and *Tomistoma* with *Gavialis* Time-scaled using the “paleotree” R package (Bapst 2012)

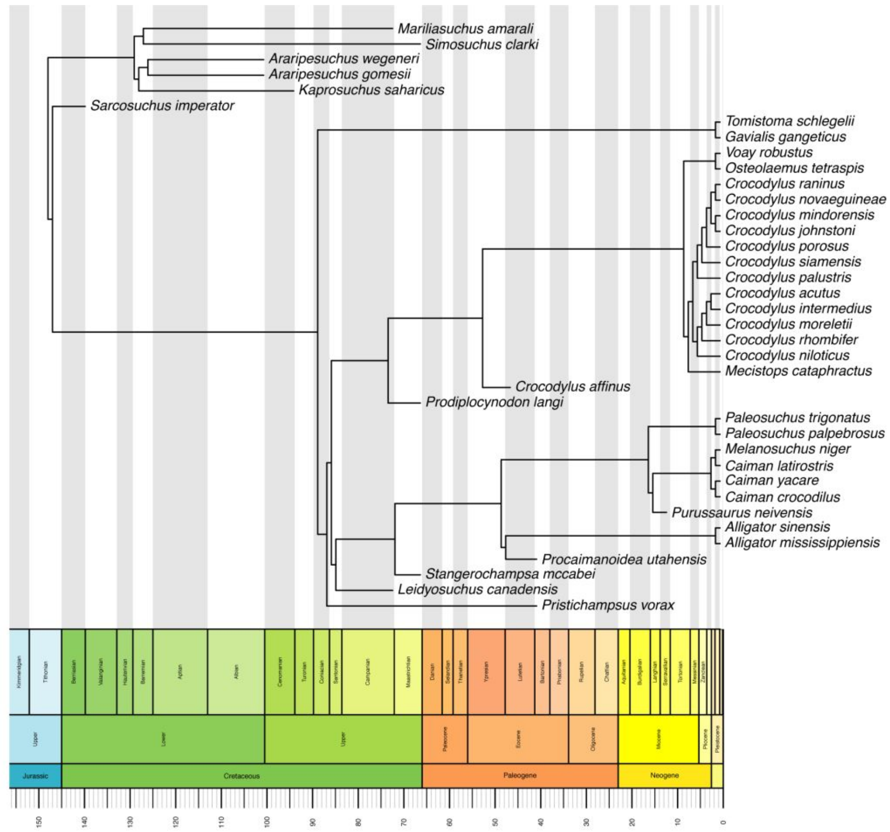

Figure S3E: Crocodylomorph hypothesis "tree 3." Thalattosuchians as neosuchians and *Tomistoma* with *Gavialis*. Time-scaled using the "paleotree" R package (Bapst 2012)

Modularity Hypotheses for Birds		
Hypothesis	Number of mo	Description
1	8	Maximally partitioned hypothesis (rostrum, palate, vault, occipital, basisphenoid, pterygoid, quadrate, naris)
2	7	Hypothesis 1 but pterygoid and quadrate joined as a single module
3	7	Hypothesis 1 but with naris and rostrum joined as a single module
4	6	Hypothesis 2 but with naris and rostrum joined as a single module
5	7	Hypothesis 1 but palate and rostrum joined as a single module
6	6	Hypothesis 1 but palate, rostrum, and naris joined as a single module
7	4	Four modules: vault, face, quadrate, and basicranium
8	3	Three modules: vault, face, and basicranium
9	2	Two modules: Face and nuerocranium
10	1	Whole skull is a single module

Modularity Hypotheses for Mesoeucrocodylians		
Hypothesis	Number of modules	Description
1	19	Maximally partitioned hypothesis
2	17	Hypothesis 1 with supraoccipital, occipital condyle, and basioccipital joined as a single module
3	17	Hypothesis 1 with frontal, parietal, and squamosal joined as a single module
4	18	Hypothesis 1 with jugal and quadrate joined as a single module
5	17	Hypothesis 1 with pterygoid, ectopterygoid, and pterygoid flange joined as a single module
6	17	Hypothesis 1 with nasal, maxilla (dorsal), and premaxilla (dorsal) joined as a single module
7	17	Hypothesis 1 with premaxilla (ventral) and premaxilla (dorsal) joined as a single module and maxilla (ventral) and maxilla (dorsal) joined as a single module
8	15	Hypothesis 2 with pterygoid, ectopterygoid, and pterygoid flange joined as a single module
9	7	Paritioned into the regions present in the bird dataset (rostrum, palate, vault, occipital, basisphenoid, pterygoid, quadrate, naris)
10	2	Two modules: face and neurocranium
11	1	Whole skull is a single module

Modularity Hypotheses for Non-avian Dinosaurs		
Hypothesis	Number of modules	Description
1	13	Maximally partitioned hypothesis
2	11	Hypothesis 1 with supraoccipital, occipital condyle, and basioccipital joined as a single module
3	11	Hypothesis 1 with frontal, parietal, and squamosal joined as a single module
4	12	Hypothesis 1 with jugal and quadrate joined as a single module
5	11	Hypothesis 1 with nasal, maxilla, and premaxilla, joined as a single module
6	3	Paritioned into the regions present in the bird dataset (rostrum, vault, occipital, quadrate)
7	2	Two modules: face and neurocranium
8	1	Whole skull is a single module

Sheet	Dataset	Phylogenetic Hypothesis	Analysis
A	Non-avian Dinosaurs, 13 regions	"Traditional" topology	EMMLi
B	Non-avian Dinosaurs, 13 regions	"Ornithoscelida" topology	EMMLi
C	Non-avian Dinosaurs, 9 regions	"Traditional" topology	EMMLi
D	Non-avian Dinosaurs, 9 regions	"Ornithoscelida" topology	EMMLi
E	Birds	Prum composite phylogen	EMMLi
F	Mesoeucrocodylians	Tree 1	EMMLi
G	Mesoeucrocodylians	Tree 2	EMMLi
H	Mesoeucrocodylians	Tree 3	EMMLi
I	Mesoeucrocodylians	Tree 4	EMMLi
J	Mesoeucrocodylians- With bird anatomical regions	Tree 1	EMMLi
K	Mesoeucrocodylians- With bird anatomical regions	Tree 2	EMMLi
L	Mesoeucrocodylians- With bird anatomical regions	Tree 3	EMMLi
M	Mesoeucrocodylians- With bird anatomical regions	Tree 4	EMMLi
O	Non-avian Dinosaurs, 13 regions	"Traditional" topology	CR
P	Non-avian Dinosaurs, 9 regions	"Traditional" topology	CR
Q	Mesoeucrocodylians	Tree 1	CR
R	Birds	Prum composite phylogen	CR

Between- and within-region correlation (ρ) from EMMLi analysis of dinosaur skulls (13 Module dataset) using traditional phylogenetic topology

	Maxilla (dorsolateral surface)	Premaxilla (dorsolateral surface)	Nasal	Frontal	Parietal	Supraoccipital	Occipital Condyle	Basioccipital	Postorbital	Jugal and Quadratojugal	Squamosal	Articular Surface of Quadrate	Prefrontal and Lacrimal
Maxilla (dorsolateral surface)	0.66	0.35	0.31	0.27	0.15	0.16	0.11	0.1	0.14	0.27	0.1	0.29	0.22
Premaxilla (dorsolateral surface)	0.35	0.64	0.37	0.36	0.24	0.1	0.05	0.12	0.12	0.15	0.09	0.15	0.18
Nasal	0.31	0.37	0.69	0.21	0.11	0.16	0.11	0.12	0.1	0.23	0.11	0.21	0.21
Frontal	0.27	0.36	0.21	0.78	0.47	0.29	0.4	0.33	0.27	0.14	0.19	0.16	0.47
Parietal	0.15	0.24	0.11	0.47	0.7	0.21	0.2	0.19	0.26	0.21	0.24	0.25	0.22
Supraocciptial	0.16	0.1	0.16	0.29	0.21	0.73	0.63	0.59	0.13	0.27	0.14	0.25	0.2
Occipital Condyle	0.11	0.05	0.11	0.4	0.2	0.63	0.97	0.86	0.12	0.14	0.08	0.23	0.29
Basioccipital	0.1	0.12	0.12	0.33	0.19	0.59	0.86	0.86	0.11	0.18	0.12	0.22	0.22
Postorbital	0.14	0.12	0.1	0.27	0.26	0.13	0.12	0.11	0.75	0.32	0.4	0.23	0.26
Jugal and Quadratojugal	0.27	0.15	0.23	0.14	0.21	0.27	0.14	0.18	0.32	0.77	0.28	0.72	0.27
Squamosal	0.1	0.09	0.11	0.19	0.24	0.14	0.08	0.12	0.4	0.28	0.63	0.31	0.19
Articular Surface of Quadrate	0.29	0.15	0.21	0.16	0.25	0.25	0.23	0.22	0.23	0.72	0.31	0.98	0.28
Prefrontal and Lacrimal	0.22	0.18	0.21	0.47	0.22	0.2	0.29	0.22	0.26	0.27	0.19	0.28	0.78

Between- and within-region correlation (ρ) from EMMLi analysis of dinosaur skulls (13-region dataset) using Ornithoscelida phylogenetic topology

	Maxilla (dorsolateral surface)	Premaxilla (dorsolateral surface)	Nasal	Frontal	Parietal	Supraoccipital	Occipital Condyle	Basioccipital	Postorbital	Jugal and Quadratojugal	Squamosal	Articular Surface of Quadrate	Prefrontal and Lacrimal
Maxilla (dorsolateral surface)	0.75	0.43	0.38	0.3	0.16	0.16	0.17	0.19	0.13	0.24	0.25	0.16	0.19
Premaxilla (dorsolateral surface)	0.43	0.65	0.47	0.33	0.18	0.13	0.23	0.24	0.11	0.25	0.22	0.17	0.16
Nasal	0.38	0.47	0.82	0.3	0.1	0.13	0.14	0.08	0.13	0.28	0.15	0.15	0.32
Frontal	0.3	0.33	0.3	0.81	0.46	0.25	0.21	0.18	0.27	0.13	0.21	0.12	0.4
Parietal	0.16	0.18	0.1	0.46	0.69	0.18	0.29	0.28	0.27	0.16	0.29	0.23	0.21
Supraocciptial	0.16	0.13	0.13	0.25	0.18	0.81	0.72	0.67	0.14	0.16	0.15	0.2	0.08
Occipital Condyle	0.17	0.23	0.14	0.21	0.29	0.72	0.98	0.92	0.14	0.07	0.19	0.24	0.08
Basioccipital	0.19	0.24	0.08	0.18	0.28	0.67	0.92	0.93	0.14	0.12	0.17	0.35	0.08
Postorbital	0.13	0.11	0.13	0.27	0.27	0.14	0.14	0.14	0.81	0.4	0.43	0.12	0.43
Jugal and Quadratojugal	0.24	0.25	0.28	0.13	0.16	0.16	0.07	0.12	0.4	0.75	0.29	0.65	0.34
Squamosal	0.25	0.22	0.15	0.21	0.29	0.15	0.19	0.17	0.43	0.29	0.72	0.19	0.18
Articular Surface of Quadrate	0.16	0.17	0.15	0.12	0.23	0.2	0.24	0.35	0.12	0.65	0.19	0.99	0.19
Prefrontal and Lacrimal	0.19	0.16	0.32	0.4	0.21	0.08	0.08	0.08	0.43	0.34	0.18	0.19	0.81

Between- and within-region correlation (ρ) from EMMLi analysis of dinosaur skulls (9-region dataset) using traditional phylogenetic topology

	Maxilla (dorsolateral surface)	Premaxilla (dorsolateral surface)	Nasal	Frontal	Parietal	Postorbital	Jugal and Quadratojugal	Squamosal	Prefrontal and Lacrimal
Maxilla (dorsolateral surface)	0.75	0.43	0.38	0.3	0.16	0.13	0.24	0.25	0.19
Premaxilla (dorsolateral surface)	0.43	0.65	0.47	0.33	0.18	0.11	0.25	0.22	0.16
Nasal	0.38	0.47	0.82	0.3	0.1	0.13	0.28	0.15	0.32
Frontal	0.3	0.33	0.3	0.81	0.46	0.27	0.13	0.21	0.4
Parietal	0.16	0.18	0.1	0.46	0.69	0.27	0.16	0.29	0.21
Postorbital	0.13	0.11	0.13	0.27	0.27	0.81	0.4	0.43	0.43
Jugal and Quadratojugal	0.24	0.25	0.28	0.13	0.16	0.4	0.75	0.29	0.34
Squamosal	0.25	0.22	0.15	0.21	0.29	0.43	0.29	0.72	0.18
Prefrontal and Lacrimal	0.19	0.16	0.32	0.4	0.21	0.43	0.34	0.18	0.81

Between- and within-region correlation (ρ) from EMMLi analysis of dinosaur skulls (9-region dataset) using Ornithoscelida phylogenetic topology

	Maxilla (dorsolateral surface)	Premaxilla (dorsolateral surface)	Nasal	Frontal	Parietal	Postorbital	Jugal and Quadratojugal	Squamosal	Prefrontal and Lacrimal
Maxilla (dorsolateral surface)	0.75	0.43	0.38	0.3	0.16	0.13	0.24	0.25	0.19
Premaxilla (dorsolateral surface)	0.43	0.65	0.47	0.33	0.18	0.11	0.25	0.22	0.16
Nasal	0.38	0.47	0.82	0.3	0.1	0.13	0.28	0.15	0.32
Frontal	0.3	0.33	0.3	0.81	0.46	0.27	0.13	0.21	0.4
Parietal	0.16	0.18	0.1	0.46	0.69	0.27	0.16	0.29	0.21
Postorbital	0.13	0.11	0.13	0.27	0.27	0.81	0.4	0.43	0.43
Jugal and Quadratojugal	0.24	0.25	0.28	0.13	0.16	0.4	0.75	0.29	0.34
Squamosal	0.25	0.22	0.15	0.21	0.29	0.43	0.29	0.72	0.18
Prefrontal and Lacrimal	0.19	0.16	0.32	0.4	0.21	0.43	0.34	0.18	0.81

Between- and within-region correlation (ρ) from EMMLi analysis of bird skulls								
	Rostrum	Vault	Basiphenoid	Palate	Pterygoid	Naris	Occipital	Quadrate
Rostrum	0.49	0.29	0.17	0.33	0.26	0.4	0.27	0.31
Vault	0.29	0.51	0.2	0.23	0.21	0.17	0.37	0.19
Basiphenoid	0.17	0.2	0.69	0.18	0.44	0.08	0.34	0.3
Palate	0.33	0.23	0.18	0.46	0.27	0.23	0.25	0.12
Pterygoid	0.26	0.21	0.44	0.27	0.87	0.11	0.23	0.69
Naris	0.4	0.17	0.08	0.23	0.11	0.77	0.14	0.06
Occipital	0.27	0.37	0.34	0.25	0.23	0.14	0.7	0.23
Quadrate	0.31	0.19	0.3	0.12	0.69	0.06	0.23	0.95

Between- and within-region correlation (ρ) from EMMLi analysis of bird skulls - Allometric effects removed								
	Rostrum	Vault	Basiphenoid	Palate	Pterygoid	Naris	Occipital	Quadrate
Rostrum	0.37	0.18	0.1	0.24	0.16	0.31	0.15	0.22
Vault	0.18	0.43	0.13	0.15	0.1	0.13	0.22	0.13
Basiphenoid	0.1	0.13	0.62	0.13	0.33	0.11	0.22	0.22
Palate	0.24	0.15	0.13	0.38	0.16	0.19	0.13	0.07
Pterygoid	0.16	0.1	0.33	0.16	0.78	0.14	0.14	0.56
Naris	0.31	0.13	0.11	0.19	0.14	0.74	0.1	0.06
Occipital	0.15	0.22	0.22	0.13	0.14	0.1	0.54	0.17
Quadrate	0.22	0.13	0.22	0.07	0.56	0.06	0.17	0.89

Between- and within-region correlation (ρ) from EMMLi analysis of Mesoeucrocodylian skulls using phylogenetic hypothesis 1 (see Electronic Supplemental Data 3)

	Premaxilla (ventral surface)	Maxilla (ventral surface)	Maxilla (dorsolateral surface)	Premaxilla (dorsolateral surface)	Nasal	Frontal	Parietal	Supraoccipital	Occipital Condyle	Basioccipital	Pterygoid	Palatine	Articular Surface of Quadrate	Jugal And Quadratojugal	Squamosal	Lacrimal and Prefrontal	Ectopterygoid	Pterygoid Flange	Postorbital and Lacrimal
Premaxilla (ventral surface)	0.87	0.43	0.37	0.74	0.34	0.25	0.11	0.21	0.24	0.06	0.22	0.42	0.39	0.2	0.15	0.37	0.18	0.1	0.15
Maxilla (ventral surface)	0.43	0.58	0.39	0.33	0.21	0.19	0.09	0.16	0.13	0.07	0.19	0.32	0.39	0.23	0.16	0.22	0.39	0.32	0.13
Maxilla (dorsolateral surface)	0.37	0.39	0.56	0.39	0.21	0.19	0.1	0.19	0.18	0.09	0.14	0.17	0.36	0.32	0.21	0.29	0.3	0.27	0.14
Premaxilla (dorsolateral surface)	0.74	0.33	0.39	0.8	0.36	0.25	0.14	0.26	0.28	0.1	0.22	0.4	0.31	0.17	0.2	0.37	0.21	0.12	0.12
Nasal	0.34	0.21	0.21	0.36	0.69	0.36	0.14	0.21	0.26	0.22	0.14	0.14	0.1	0.1	0.13	0.43	0.11	0.12	0.16
Frontal	0.25	0.19	0.19	0.25	0.36	0.75	0.34	0.23	0.27	0.19	0.12	0.1	0.17	0.15	0.24	0.56	0.07	0.09	0.45
Parietal	0.11	0.09	0.1	0.14	0.14	0.34	0.7	0.4	0.22	0.15	0.23	0.17	0.19	0.12	0.4	0.22	0.18	0.28	0.35
Supraoccipital	0.21	0.16	0.19	0.26	0.21	0.23	0.4	0.65	0.57	0.37	0.14	0.15	0.26	0.18	0.36	0.34	0.12	0.14	0.1
Occipital Condyle	0.24	0.13	0.18	0.28	0.26	0.27	0.22	0.57	0.91	0.6	0.16	0.13	0.06	0.14	0.2	0.4	0.1	0.13	0.19
Basioccipital	0.06	0.07	0.09	0.1	0.22	0.19	0.15	0.37	0.6	0.75	0.32	0.14	0.12	0.13	0.16	0.27	0.12	0.09	0.18
Pterygoid	0.22	0.19	0.14	0.22	0.14	0.12	0.23	0.14	0.16	0.32	0.69	0.4	0.18	0.12	0.23	0.11	0.42	0.51	0.21
Palatine	0.42	0.32	0.17	0.4	0.14	0.1	0.17	0.15	0.13	0.14	0.4	0.73	0.12	0.1	0.2	0.18	0.3	0.2	0.12
Articular Surface of Quadrate	0.39	0.39	0.36	0.31	0.1	0.17	0.19	0.26	0.06	0.12	0.18	0.12	0.95	0.44	0.25	0.14	0.37	0.43	0.09
Jugal And Quadratojugal	0.2	0.23	0.32	0.17	0.1	0.15	0.12	0.18	0.14	0.13	0.12	0.1	0.44	0.6	0.27	0.23	0.29	0.23	0.29
Squamosal	0.15	0.16	0.21	0.2	0.13	0.24	0.4	0.36	0.2	0.16	0.23	0.2	0.25	0.27	0.63	0.22	0.16	0.2	0.43
Lacrimal and Prefrontal	0.37	0.22	0.29	0.37	0.43	0.56	0.22	0.34	0.4	0.27	0.11	0.18	0.14	0.23	0.22	0.8	0.1	0.08	0.3
Ectopterygoid	0.18	0.39	0.3	0.21	0.11	0.07	0.18	0.12	0.1	0.12	0.42	0.3	0.37	0.29	0.16	0.1	0.76	0.65	0.16
Pterygoid Flange	0.1	0.32	0.27	0.12	0.12	0.09	0.28	0.14	0.13	0.09	0.51	0.2	0.43	0.23	0.2	0.08	0.65	0.94	0.18
Postorbital and Lacrimal	0.15	0.13	0.14	0.12	0.16	0.45	0.35	0.1	0.19	0.18	0.21	0.12	0.09	0.29	0.43	0.3	0.16	0.18	0.7

Between- and within-region correlation (ρ) from EMMLi analysis of Mesoeucrocodylian skulls - Allometric effects removed- using phylogenetic hypothesis 1 (see Electronic Supplemental Data 2)

	Premaxilla (ventral surface)	Maxilla (ventral surface)	Maxilla (dorsolateral surface)	Premaxilla (dorsolateral surface)	Nasal	Frontal	Parietal	Supraoccipital	Occipital Condyle	Basioccipital	Pterygoid	Palatine	Articular Surface of Quadrate	Jugal And Quadratojugal	Squamosal	Lacrimal and Prefrontal	Ectopterygoid	Pterygoid Flange	Postorbital and Lacrimal
Premaxilla (ventral surface)	0.87	0.39	0.37	0.78	0.22	0.15	0.1	0.22	0.12	0.15	0.36	0.38	0.34	0.21	0.2	0.24	0.28	0.13	0.07
Maxilla (ventral surface)	0.39	0.57	0.39	0.33	0.17	0.19	0.22	0.18	0.1	0.1	0.28	0.39	0.42	0.27	0.18	0.14	0.46	0.41	0.15
Maxilla (dorsolateral surface)	0.37	0.39	0.57	0.41	0.18	0.2	0.2	0.23	0.15	0.08	0.25	0.23	0.4	0.36	0.24	0.24	0.38	0.36	0.18
Premaxilla (dorsolateral surface)	0.78	0.33	0.41	0.85	0.25	0.16	0.12	0.3	0.18	0.11	0.4	0.39	0.26	0.2	0.28	0.28	0.32	0.17	0.1
Nasal	0.22	0.17	0.18	0.25	0.64	0.37	0.24	0.2	0.09	0.1	0.23	0.18	0.14	0.13	0.27	0.28	0.2	0.24	0.22
Frontal	0.15	0.19	0.2	0.16	0.37	0.8	0.5	0.2	0.09	0.11	0.18	0.15	0.26	0.13	0.34	0.5	0.17	0.22	0.51
Parietal	0.1	0.22	0.2	0.12	0.24	0.5	0.78	0.42	0.19	0.15	0.33	0.25	0.34	0.13	0.5	0.15	0.32	0.42	0.46
Supraoccipital	0.22	0.18	0.23	0.3	0.2	0.2	0.42	0.66	0.46	0.29	0.27	0.19	0.29	0.21	0.48	0.15	0.2	0.23	0.25
Occipital Condyle	0.12	0.1	0.15	0.18	0.09	0.09	0.19	0.46	0.85	0.5	0.15	0.1	0.12	0.21	0.16	0.13	0.14	0.21	0.11
Basioccipital	0.15	0.1	0.08	0.11	0.1	0.11	0.15	0.29	0.5	0.73	0.3	0.18	0.17	0.14	0.13	0.09	0.13	0.11	0.12
Pterygoid	0.36	0.28	0.25	0.4	0.23	0.18	0.33	0.27	0.15	0.3	0.76	0.49	0.18	0.19	0.37	0.11	0.55	0.58	0.31
Palatine	0.38	0.39	0.23	0.39	0.18	0.15	0.25	0.19	0.1	0.18	0.49	0.75	0.08	0.18	0.27	0.13	0.45	0.37	0.2
Articular Surface of Quadrate	0.34	0.42	0.4	0.26	0.14	0.26	0.34	0.29	0.12	0.17	0.18	0.08	0.95	0.5	0.23	0.13	0.42	0.51	0.15
Jugal And Quadratojugal	0.21	0.27	0.36	0.2	0.13	0.13	0.13	0.21	0.21	0.14	0.19	0.18	0.5	0.62	0.26	0.22	0.35	0.33	0.28
Squamosal	0.2	0.18	0.24	0.28	0.27	0.34	0.5	0.48	0.16	0.13	0.37	0.27	0.23	0.26	0.7	0.18	0.21	0.24	0.51
Lacrimal and Prefrontal	0.24	0.14	0.24	0.28	0.28	0.5	0.15	0.15	0.13	0.09	0.11	0.13	0.13	0.22	0.18	0.71	0.14	0.14	0.29
Ectopterygoid	0.28	0.46	0.38	0.32	0.2	0.17	0.32	0.2	0.14	0.13	0.55	0.45	0.42	0.35	0.21	0.14	0.82	0.73	0.2
Pterygoid Flange	0.13	0.41	0.36	0.17	0.24	0.22	0.42	0.23	0.21	0.11	0.58	0.37	0.51	0.33	0.24	0.14	0.73	0.95	0.23
Postorbital and Lacrimal	0.07	0.15	0.18	0.1	0.22	0.51	0.46	0.25	0.11	0.12	0.31	0.2	0.15	0.28	0.51	0.29	0.2	0.23	0.7

Between- and within-region correlation (ρ) from EMMLi analysis of Mesoeucrocodylian skulls using phylogenetic hypothesis 2 (see Electronic Supplemental Data 3)

	Premaxilla (ventral surface)	Maxilla (ventral surface)	Maxilla (dorsolateral surface)	Premaxilla (dorsolateral surface)	Nasal	Frontal	Parietal	Supraoccipital	Occipital Condyle	Basioccipital	Pterygoid	Palatine	Articular Surface of Quadrate	Jugal And Quadratojugal	Squamosal	Lacrimal and Prefrontal	Ectopterygoid	Pterygoid Flange	Postorbital and Lacrimal
Premaxilla (ventral surface)	0.87	0.43	0.37	0.74	0.34	0.26	0.1	0.2	0.23	0.06	0.21	0.4	0.39	0.2	0.14	0.36	0.17	0.1	0.17
Maxilla (ventral surface)	0.43	0.58	0.39	0.33	0.22	0.19	0.09	0.16	0.13	0.07	0.18	0.3	0.39	0.23	0.16	0.22	0.38	0.33	0.14
Maxilla (dorsolateral surface)	0.37	0.39	0.56	0.39	0.21	0.19	0.1	0.19	0.18	0.09	0.14	0.16	0.37	0.33	0.21	0.29	0.3	0.27	0.15
Premaxilla (dorsolateral surface)	0.74	0.33	0.39	0.8	0.35	0.26	0.13	0.24	0.27	0.1	0.21	0.38	0.31	0.17	0.19	0.37	0.2	0.14	0.15
Nasal	0.34	0.22	0.21	0.35	0.69	0.36	0.14	0.21	0.26	0.23	0.15	0.14	0.1	0.11	0.14	0.42	0.12	0.11	0.17
Frontal	0.26	0.19	0.19	0.26	0.36	0.75	0.34	0.23	0.28	0.19	0.12	0.1	0.16	0.16	0.24	0.57	0.07	0.09	0.45
Parietal	0.1	0.09	0.1	0.13	0.14	0.34	0.69	0.39	0.22	0.15	0.22	0.15	0.19	0.12	0.39	0.22	0.17	0.29	0.34
Supraoccipital	0.2	0.16	0.19	0.24	0.21	0.23	0.39	0.64	0.57	0.38	0.13	0.13	0.26	0.18	0.35	0.34	0.12	0.16	0.11
Occipital Condyle	0.23	0.13	0.18	0.27	0.26	0.28	0.22	0.57	0.91	0.6	0.17	0.13	0.06	0.14	0.2	0.4	0.1	0.14	0.21
Basioccipital	0.06	0.07	0.09	0.1	0.23	0.19	0.15	0.38	0.6	0.75	0.32	0.14	0.12	0.13	0.16	0.28	0.12	0.09	0.19
Pterygoid	0.21	0.18	0.14	0.21	0.15	0.12	0.22	0.13	0.17	0.32	0.68	0.39	0.18	0.11	0.21	0.11	0.41	0.55	0.19
Palatine	0.4	0.3	0.16	0.38	0.14	0.1	0.15	0.13	0.13	0.14	0.39	0.71	0.12	0.1	0.19	0.17	0.29	0.23	0.11
Articular Surface of Quadrate	0.39	0.39	0.37	0.31	0.1	0.16	0.19	0.26	0.06	0.12	0.18	0.12	0.95	0.44	0.25	0.14	0.37	0.44	0.09
Jugal And Quadratojugal	0.2	0.23	0.33	0.17	0.11	0.16	0.12	0.18	0.14	0.13	0.11	0.1	0.44	0.6	0.27	0.23	0.3	0.23	0.29
Squamosal	0.14	0.16	0.21	0.19	0.14	0.24	0.39	0.35	0.2	0.16	0.21	0.19	0.25	0.27	0.63	0.22	0.16	0.21	0.43
Lacrimal and Prefrontal	0.36	0.22	0.29	0.37	0.42	0.57	0.22	0.34	0.4	0.28	0.11	0.17	0.14	0.23	0.22	0.8	0.1	0.08	0.32
Ectopterygoid	0.17	0.38	0.3	0.2	0.12	0.07	0.17	0.12	0.1	0.12	0.41	0.29	0.37	0.3	0.16	0.1	0.75	0.68	0.16
Pterygoid Flange	0.1	0.33	0.27	0.14	0.11	0.09	0.29	0.16	0.14	0.09	0.55	0.23	0.44	0.23	0.21	0.08	0.68	0.94	0.18
Postorbital and Lacrimal	0.17	0.14	0.15	0.15	0.17	0.45	0.34	0.11	0.21	0.19	0.19	0.11	0.09	0.29	0.43	0.32	0.16	0.18	0.7

Between- and within-region correlation (ρ) from EMMLi analysis of Mesoeucrocodylian skulls using phylogenetic hypothesis 3 (see Electronic Supplemental Data 3)

	Premaxilla (ventral surface)	Maxilla (ventral surface)	Maxilla (dorsolateral surface)	Premaxilla (dorsolateral surface)	Nasal	Frontal	Parietal	Supraoccipital	Occipital Condyle	Basioccipital	Pterygoid	Palatine	Articular Surface of Quadrate	Jugal And Quadratojugal	Squamosal	Lacrimal and Prefrontal	Ectopterygoid	Pterygoid Flange	Postorbital and Lacrimal
Premaxilla (ventral surface)	0.86	0.42	0.29	0.66	0.28	0.27	0.1	0.2	0.27	0.08	0.2	0.34	0.35	0.19	0.13	0.32	0.16	0.1	0.18
Maxilla (ventral surface)	0.42	0.58	0.35	0.28	0.19	0.22	0.1	0.14	0.15	0.11	0.18	0.3	0.31	0.2	0.15	0.21	0.37	0.31	0.17
Maxilla (dorsolateral surface)	0.29	0.35	0.54	0.38	0.2	0.18	0.12	0.18	0.13	0.09	0.13	0.19	0.37	0.3	0.21	0.27	0.28	0.25	0.14
Premaxilla (dorsolateral surface)	0.66	0.28	0.38	0.78	0.34	0.22	0.15	0.25	0.25	0.12	0.2	0.38	0.34	0.18	0.24	0.33	0.2	0.14	0.12
Nasal	0.28	0.19	0.2	0.34	0.7	0.29	0.14	0.17	0.16	0.13	0.13	0.17	0.12	0.09	0.1	0.37	0.11	0.1	0.11
Frontal	0.27	0.22	0.18	0.22	0.29	0.74	0.33	0.23	0.29	0.22	0.11	0.09	0.13	0.16	0.27	0.54	0.07	0.08	0.48
Parietal	0.1	0.1	0.12	0.15	0.14	0.33	0.69	0.39	0.22	0.15	0.2	0.16	0.18	0.13	0.35	0.2	0.18	0.29	0.32
Supraoccipital	0.2	0.14	0.18	0.25	0.17	0.23	0.39	0.64	0.56	0.38	0.13	0.13	0.28	0.17	0.34	0.32	0.12	0.16	0.13
Occipital Condyle	0.27	0.15	0.13	0.25	0.16	0.29	0.22	0.56	0.92	0.64	0.18	0.09	0.1	0.14	0.19	0.35	0.11	0.15	0.24
Basioccipital	0.08	0.11	0.09	0.12	0.13	0.22	0.15	0.38	0.64	0.77	0.33	0.17	0.18	0.14	0.16	0.24	0.11	0.08	0.23
Pterygoid	0.2	0.18	0.13	0.2	0.13	0.11	0.2	0.13	0.18	0.33	0.68	0.39	0.17	0.12	0.19	0.1	0.4	0.53	0.18
Palatine	0.34	0.3	0.19	0.38	0.17	0.09	0.16	0.13	0.09	0.17	0.39	0.71	0.16	0.11	0.22	0.15	0.28	0.22	0.13
Articular Surface of Quadrate	0.35	0.31	0.37	0.34	0.12	0.13	0.18	0.28	0.1	0.18	0.17	0.16	0.95	0.44	0.26	0.14	0.35	0.42	0.08
Jugal And Quadratojugal	0.19	0.2	0.3	0.18	0.09	0.16	0.13	0.17	0.14	0.14	0.12	0.11	0.44	0.59	0.29	0.22	0.29	0.22	0.3
Squamosal	0.13	0.15	0.21	0.24	0.1	0.27	0.35	0.34	0.19	0.16	0.19	0.22	0.26	0.29	0.67	0.21	0.15	0.18	0.51
Lacrimal and Prefrontal	0.32	0.21	0.27	0.33	0.37	0.54	0.2	0.32	0.35	0.24	0.1	0.15	0.14	0.22	0.21	0.78	0.1	0.08	0.31
Ectopterygoid	0.16	0.37	0.28	0.2	0.11	0.07	0.18	0.12	0.11	0.11	0.4	0.28	0.35	0.29	0.15	0.1	0.75	0.67	0.15
Pterygoid Flange	0.1	0.31	0.25	0.14	0.1	0.08	0.29	0.16	0.15	0.08	0.53	0.22	0.42	0.22	0.18	0.08	0.67	0.94	0.16
Postorbital and Lacrimal	0.18	0.17	0.14	0.12	0.11	0.48	0.32	0.13	0.24	0.23	0.18	0.13	0.08	0.3	0.51	0.31	0.15	0.16	0.74

Between- and within-region correlation (ρ) from EMMLi analysis of Mesoeucrocodylian skulls using phylogenetic hypothesis 4 (see Electronic Supplemental Data 3)

	Premaxilla (ventral surface)	Maxilla (ventral surface)	Maxilla (dorsolateral surface)	Premaxilla (dorsolateral surface)	Nasal	Frontal	Parietal	Supraoccipital	Occipital Condyle	Basioccipital	Pterygoid	Palatine	Articular Surface of Quadrate	Jugal And Quadratojugal	Squamosal	Lacrimal and Prefrontal	Ectopterygoid	Pterygoid Flange	Postorbital and Lacrimal
Premaxilla (ventral surface)	0.86	0.41	0.29	0.67	0.28	0.26	0.1	0.21	0.28	0.08	0.21	0.36	0.35	0.18	0.14	0.33	0.17	0.1	0.16
Maxilla (ventral surface)	0.41	0.58	0.35	0.28	0.18	0.21	0.11	0.14	0.15	0.1	0.19	0.31	0.31	0.2	0.15	0.21	0.37	0.3	0.17
Maxilla (dorsolateral surface)	0.29	0.35	0.54	0.37	0.2	0.18	0.11	0.18	0.13	0.09	0.14	0.2	0.37	0.3	0.21	0.27	0.28	0.25	0.14
Premaxilla (dorsolateral surface)	0.67	0.28	0.37	0.79	0.34	0.21	0.16	0.27	0.26	0.12	0.22	0.4	0.33	0.17	0.25	0.33	0.21	0.12	0.1
Nasal	0.28	0.18	0.2	0.34	0.7	0.29	0.14	0.17	0.16	0.12	0.12	0.17	0.13	0.09	0.11	0.37	0.1	0.11	0.11
Frontal	0.26	0.21	0.18	0.21	0.29	0.74	0.33	0.23	0.29	0.21	0.12	0.09	0.13	0.16	0.27	0.54	0.07	0.08	0.48
Parietal	0.1	0.11	0.11	0.16	0.14	0.33	0.69	0.4	0.22	0.15	0.21	0.17	0.18	0.13	0.36	0.2	0.19	0.28	0.33
Supraoccipital	0.21	0.14	0.18	0.27	0.17	0.23	0.4	0.64	0.56	0.37	0.14	0.14	0.27	0.17	0.35	0.32	0.12	0.14	0.12
Occipital Condyle	0.28	0.15	0.13	0.26	0.16	0.29	0.22	0.56	0.91	0.63	0.17	0.09	0.1	0.14	0.19	0.36	0.11	0.14	0.23
Basioccipital	0.08	0.1	0.09	0.12	0.12	0.21	0.15	0.37	0.63	0.77	0.33	0.17	0.18	0.14	0.16	0.24	0.11	0.08	0.22
Pterygoid	0.21	0.19	0.14	0.22	0.12	0.12	0.21	0.14	0.17	0.33	0.68	0.4	0.17	0.12	0.2	0.1	0.4	0.49	0.19
Palatine	0.36	0.31	0.2	0.4	0.17	0.09	0.17	0.14	0.09	0.17	0.4	0.72	0.16	0.12	0.23	0.16	0.29	0.2	0.14
Articular Surface of Quadrate	0.35	0.31	0.37	0.33	0.13	0.13	0.18	0.27	0.1	0.18	0.17	0.16	0.95	0.44	0.26	0.14	0.34	0.42	0.08
Jugal And Quadratojugal	0.18	0.2	0.3	0.17	0.09	0.16	0.13	0.17	0.14	0.14	0.12	0.12	0.44	0.59	0.29	0.22	0.29	0.22	0.3
Squamosal	0.14	0.15	0.21	0.25	0.11	0.27	0.36	0.35	0.19	0.16	0.2	0.23	0.26	0.29	0.67	0.21	0.15	0.18	0.51
Lacrimal and Prefrontal	0.33	0.21	0.27	0.33	0.37	0.54	0.2	0.32	0.36	0.24	0.1	0.16	0.14	0.22	0.21	0.78	0.1	0.08	0.3
Ectopterygoid	0.17	0.37	0.28	0.21	0.1	0.07	0.19	0.12	0.11	0.11	0.4	0.29	0.34	0.29	0.15	0.1	0.75	0.65	0.15
Pterygoid Flange	0.1	0.3	0.25	0.12	0.11	0.08	0.28	0.14	0.14	0.08	0.49	0.2	0.42	0.22	0.18	0.08	0.65	0.93	0.16
Postorbital and Lacrimal	0.16	0.17	0.14	0.1	0.11	0.48	0.33	0.12	0.23	0.22	0.19	0.14	0.08	0.3	0.51	0.3	0.15	0.16	0.74

Between- and within-region correlation (ρ) from EMMLi analysis of Mesoeucrocodylian skulls with landmarks partitioned into the regeions present in birds using phylogenetic hypothesis 1 (see Electronic Supplemental Data 3)							
	Rostrum	Vault	Palate	Pterygoid	Naris	Occipital	Quadrate
Rostrum	0.37	0.22	0.28	0.19	0.35	0.18	0.32
Vault	0.22	0.46	0.17	0.16	0.17	0.26	0.16
Palate	0.28	0.17	0.5	0.28	0.43	0.14	0.31
Pterygoid	0.19	0.16	0.28	0.61	0.28	0.15	0.3
Naris	0.35	0.17	0.43	0.28	0.86	0.16	0.23
Occipital	0.18	0.26	0.14	0.15	0.16	0.6	0.16
Quadrate	0.32	0.16	0.31	0.3	0.23	0.16	0.94

Between- and within-region correlation (ρ) from EMMLi analysis of Mesoeucrocodylian skulls with landmarks partitioned into the regeions present in birds using phylogenetic hypothesis 2 (see Electronic Supplemental Data 3)							
	Rostrum	Vault	Palate	Pterygoid	Naris	Occipital	Quadrate
Rostrum	0.38	0.2	0.29	0.21	0.34	0.17	0.34
Vault	0.2	0.45	0.16	0.15	0.16	0.26	0.17
Palate	0.29	0.16	0.48	0.29	0.4	0.14	0.32
Pterygoid	0.21	0.15	0.29	0.62	0.27	0.15	0.32
Naris	0.34	0.16	0.4	0.27	0.86	0.15	0.24
Occipital	0.17	0.26	0.14	0.15	0.15	0.59	0.17
Quadrate	0.34	0.17	0.32	0.32	0.24	0.17	0.94

Between- and within-region correlation (ρ) from EMMLi analysis of Mesoeucrocodylian skulls with landmarks partitioned into the regeions present in birds using phylogenetic hypothesis 3 (see Electronic Supplemental Data 3)

	Rostrum	Vault	Palate	Pterygoid	Naris	Occipital	Quadrate
Rostrum	0.36	0.21	0.26	0.17	0.37	0.16	0.32
Vault	0.21	0.45	0.18	0.14	0.18	0.25	0.16
Palate	0.26	0.18	0.48	0.27	0.37	0.14	0.29
Pterygoid	0.17	0.14	0.27	0.59	0.24	0.16	0.28
Naris	0.37	0.18	0.37	0.24	0.85	0.16	0.32
Occipital	0.16	0.25	0.14	0.16	0.16	0.58	0.21
Quadrate	0.32	0.16	0.29	0.28	0.32	0.21	0.96

Between- and within-region correlation (ρ) from EMMLi analysis of Mesoeucrocodylian skulls with landmarks partitioned into the regeions present in birds using phylogenetic hypothesis 4 (see Electronic Supplemental Data 3)

	Rostrum	Vault	Palate	Pterygoid	Naris	Occipital	Quadrate
Rostrum	0.36	0.2	0.26	0.18	0.34	0.17	0.35
Vault	0.2	0.45	0.18	0.14	0.18	0.25	0.17
Palate	0.26	0.18	0.49	0.25	0.38	0.15	0.28
Pterygoid	0.18	0.14	0.25	0.6	0.24	0.16	0.29
Naris	0.34	0.18	0.38	0.24	0.85	0.17	0.3
Occipital	0.17	0.25	0.15	0.16	0.17	0.59	0.21
Quadrate	0.35	0.17	0.28	0.29	0.3	0.21	0.95

Pairwise Covariance Ratios - Non-avian Dinosaurs- 13-Region Dataset ("Traditional" Phylogenetic Hypothesis)												
	Maxilla (dorsolateral surface)	Premaxilla (dorsolateral surface)	Nasal	Frontal	Parietal	Supraoccipital	Occipital Condyle	Basioccipital	Postorbital	Jugal and Quadratojugal	Squamosal	Articular Surface of Quadrate
Premaxilla (dorsolateral surface)	0.86											
Nasal	0.80	0.86										
Frontal	0.57	0.72	0.55									
Parietal	0.47	0.59	0.43	0.86								
Supraocciptial	0.56	0.61	0.49	0.78	0.73							
Occipital Condyle	0.58	0.46	0.38	0.66	0.68	0.82						
Basioccipital	0.59	0.53	0.39	0.73	0.74	0.84	0.97					
Postorbital	0.57	0.65	0.52	0.84	0.77	0.70	0.48	0.55				
Jugal and Quadratojugal	0.72	0.76	0.65	0.80	0.81	0.78	0.57	0.63	0.85			
Squamosal	0.49	0.60	0.46	0.74	0.77	0.68	0.40	0.57	0.83	0.77		
Articular Surface of Quadrate	0.60	0.67	0.54	0.78	0.82	0.69	0.52	0.61	0.74	0.92	0.69	
Prefrontal and Lacrimal	0.55	0.68	0.48	0.85	0.78	0.76	0.60	0.68	0.72	0.83	0.70	0.79

Pairwise Covariance Ratios - Non-avian Dinosaurs- 9-Region Dataset ("Traditional" Phylogenetic Hypothesis)								
	Maxilla (dorsolateral surface)	Premaxilla (dorsolateral surface)	Nasal	Frontal	Parietal	Postorbital	Jugal and Quadratojugal	Squamosal
Premaxilla (dorsolateral surface)	0.92							
Nasal	0.93	0.93						
Frontal	0.86	0.83	0.85					
Parietal	0.90	0.88	0.86	0.96				
Postorbital	0.87	0.87	0.86	0.87	0.87			
Jugal and Quadratojugal	0.82	0.78	0.82	0.91	0.88	0.93		
Squamosal	0.91	0.90	0.88	0.87	0.88	0.87	0.83	
Prefrontal and Lacrimal	0.96	0.94	0.96	0.83	0.87	0.87	0.82	0.90

Pairwise Covariance Ratios - Mesoeucrocodylians (Phylogenetic Hypothesis 1)																		
	Premaxilla (ventral surface)	Maxilla (ventral surface)	Maxilla (dorsolateral surface)	Premaxilla (dorsolateral surface)	Nasal	Frontal	Parietal	Supraoccipital	Occipital Condyle	Basioccipital	Pterygoid	Palatine	Articular Surface of Quadrate	Jugal And Quadratojugal	Squamosal	Lacrimal and Prefrontal	Ectopterygoid	Pterygoid Flange
Maxilla (ventral surface)	0.91																	
Maxilla (dorsolateral surface)	0.91	0.93																
Premaxilla (dorsolateral surface)	0.95	0.83	0.89															
Nasal	0.55	0.53	0.50	0.60														
Frontal	0.63	0.58	0.59	0.66	0.57													
Parietal	0.58	0.51	0.55	0.65	0.52	0.84												
Supraoccipital	0.60	0.59	0.59	0.62	0.54	0.76	0.85											
Occipital Condyle	0.45	0.46	0.42	0.48	0.50	0.65	0.63	0.84										
Basioccipital	0.47	0.55	0.50	0.43	0.48	0.56	0.51	0.72	0.78									
Pterygoid	0.78	0.80	0.79	0.74	0.46	0.58	0.59	0.59	0.39	0.62								
Palatine	0.72	0.78	0.70	0.68	0.39	0.48	0.52	0.50	0.41	0.40	0.72							
Articular Surface of Quadrate	0.75	0.79	0.76	0.68	0.44	0.48	0.46	0.62	0.29	0.63	0.79	0.54						
Jugal And Quadratojugal	0.80	0.83	0.86	0.79	0.55	0.63	0.61	0.72	0.53	0.58	0.73	0.58	0.84					
Squamosal	0.78	0.74	0.73	0.75	0.48	0.81	0.83	0.81	0.63	0.60	0.77	0.61	0.74	0.79				
Lacrimal and Prefrontal	0.60	0.57	0.64	0.66	0.56	0.89	0.84	0.84	0.69	0.58	0.52	0.47	0.44	0.71	0.80			
Ectopterygoid	0.80	0.89	0.88	0.79	0.47	0.47	0.53	0.59	0.31	0.52	0.82	0.59	0.86	0.86	0.71	0.48		
Pterygoid Flange	0.77	0.83	0.82	0.74	0.41	0.49	0.55	0.60	0.34	0.52	0.86	0.59	0.83	0.79	0.72	0.49	0.93	
Postorbital and Lacrimal	0.75	0.68	0.70	0.76	0.50	0.86	0.79	0.73	0.65	0.63	0.69	0.57	0.58	0.77	0.90	0.82	0.63	0.60

Pairwise Covariance Ratios - Birds							
	Rostrum	Vault	Basiphenoid	Palate	Pterygoid	Naris	Occipital
Vault	0.82						
Basiphenoid	0.59	0.64					
Palate	0.93	0.79	0.60				
Pterygoid	0.67	0.68	0.73	0.64			
Naris	0.70	0.39	0.29	0.50	0.40		
Occipital	0.72	0.83	0.69	0.73	0.62	0.33	
Quadrate	0.70	0.69	0.63	0.64	0.86	0.41	0.64